Research Square

Preprints are preliminary reports that have not undergone peer review. They should not be considered conclusive, used to inform clinical practice, or referenced by the media as validated information.

Conversions of Cement bypass waste to Nano-hydroxyapatite exploited in water purification

Safaa El-Nahas
South Valley University Faculty of Science

Adilla ElSaadi Mohamed
Aswan University

Randa Roshdy Ahmed
Aswan University

Mahmoud Sayed Abd El-sadek (mahmoud.abdelsadek@sci.svu.edu.eg)
South Valley University Faculty of Science https://orcid.org/0000-0002-6640-7845

Research Article

Keywords: cement bypass dust, nano-hydroxyapatite, removal of Fe3+ Mn2+

Posted Date: September 15th, 2022

DOI: https://doi.org/10.21203/rs.3.rs-1871491/v1

License: This work is licensed under a Creative Commons Attribution 4.0 International License.
Read Full License

Abstract

The goal of this study is to convert cement bypass dust into a usable product called hydroxyapatite. Four hydroxyapatites' samples (Kiln-HA1- Kiln-HA4) were successfully prepared in nano-scale (14.8–25.7 nm). The specific surface areas of all of the samples examined were high: Kiln-HA3 (161.5 m^2/g) > Kiln-HA1 (130.2 m^2/g) > Kiln-HA2 (81.9 m^2/g) > Kiln-HA4 (54.1 m^2/g).Tested nano- hydroxyapatite successfully removed Fe^{3+} and Mn^{2+} as pollutants from water with efficiencies of up to 95% for both Fe and Mn ions. The maximum adsorption capacities (q_{max}) of nano hydroxyapatite varied from 147 to 175 $mg.g^{-1}$ for adsorbed Fe (III), while were wide ranged from 204 to 344 $mg.g^{-1}$ for adsorbed Mn (II).Hydroxyapatite-selectivity for removing Mn and Fe ions in mixed solutions was as follows: Fe^{3+}> Cu^{2+}>Mn^{2+}. In multiple cycles, the investigated materials were able to remove Fe and Mn ions without regeneration. The overall cost of producing 100 grams of hydroxyapatite from cement bypass waste is less than other calcium source which was 184 EGP/100g (9.32 €/100g).

Introduction

The uses of alternative eco- friendly techniques for reducing or remedial number of industrial wastes have been gradually gaining global attention from regulatory agencies. Physical and chemical analysis of waste materials can assist to expand the range of useful applications for these wastes (Peters, 1998). Manufacturing of cement is considered one of the most strategic industries that are directly related to the construction and building works that playing an important role in the development the country's economy. Cement is mainly used as a hydraulic bond material in building materials. Portland cement consists of a mixture of limestone and clay minerals (Zeb et al., 2019). Cement dust is one of the most harmful pollutants that harm the environment and human health. During the cement manufacturing process, large varieties of different dusts are released as cement kiln dust and bypass as byproducts (Czapik et al., 2020). The proportion of overall cement kiln dust that is used as raw feed material in cement manufacturing ranges from 64–73% (Peethamparan et al., 2008). The cement bypass dust (CBPD) is not the classical cement kiln dust (CKD) and differ in their composition (Zeb et al., 2019). CKD is the mixture of dusts produced during manufacturing cement that consists of unreacted raw feed and calcinated clinker dust with contents of some alkali halides or sulfates and presence of volatiles materials. While, cement bypass dust (CBPD) is the final byproduct of cement dust that is distinguished by high content of chlorides, potassium and sulfate make it rejected to be re-used as raw feed materials like(CKD) (Czapik et al., 2020; Zeb et al., 2019). As a result, the cement bypass waste had a higher concentration of chlorine, alkalis, and sulfur than CKD waste (Roth, 2015). Huge amounts (54–200 kg) of waste were created during the production of one tons of cement clinker (Sultan et al., 2018). Egyptian cement factories emit between 200 and 300 tons of dust per day, accounting for 10–17% of dry process cement output (Peethamparan et al., 2008). To avoid deposition hazards, CKD and CBPD dust are treated with water to give it a hard shape that makes it simpler to carry and handle (Roth, 2015). The chemical composition of CBPD waste is significantly depend on various factors as raw material feed, source of fuel, kiln temperature and dust collection systems (Peethamparan et al., 2008; Roth, 2015). Only a little amount of cement bypass(

around 6%) had any sort of application (Peethamparan et al., 2008). Cement bypass waste is beneficially utilized in a variety ways, including soil stabilization, waste treatment, asphalt concrete filing, and pozzolanic base stabilization (Peethamparan et al., 2008), composite materials (Ibrahim et al., 2020), synthesizing of geopolymer (Abdulaziz et al., 2013), and microbiological application in wastewater treatment (Ahmad et al., 2019). Egypt's government is concerned about water security and may turn to groundwater as a viable supply alongside the Nile River for drinking and agricultural purposes. The "New Valley Project" and the "South Egypt Development Project" are excellent examples of deserts reclaiming land in order to meet growing food demands; however the sustainability of such agricultural activities is entirely contingent on the availability of reliable water sources (Han et al., 2017). The majority of villages in Delta governorates rely on groundwater for drinking and agriculture (Alothman, 2012). Iron and manganese (Mn^{2+} and Fe^{3+}) are typically present in dissolved form as ions in ordinary groundwater. These ions must be eliminated to avoid discoloration of treated water or mineral oxide build-up in the pipeline(El-Nahas, Safaa et al., 2020). In situations of high Fe(II) or Mn(II) concentrations in groundwater, strong oxidising agents such as calcium hypochlorite salts Ca $(OCl)_2$, NaOCl, and KMnO4 are already used to accomplish the necessary quick oxidation process (Alothman, 2012),(El-Nahas, Safaa et al., 2020). The downside of employing $KMnO_4$ as an oxidant is that even a tiny amount turns the treated water pink. Adsorption has shown to be a successful approach for removing a wide range of contaminants from water (Abdel Maksoud et al., 2020). Nano-adsorbents are particularly successful in eliminating a wide range of contaminants because to their high specific surface area, porosity, and active surface sites (Abdel Maksoud et al., 2020). Hydroxyapatite $Ca_{10}(PO_4)_6(OH)_2$ is an useful adsorbent material for removing pollutants due to its high sorption capacity, cheap price, and high stability under oxidizing and reducing processes (El-Nahas, Safaa et al., 2020). Hydroxyapatite is regarded as an ecologically friendly material for a variety of reasons, including its absence of toxicity and biocompatibility. As well as a number of other professions that contributes to the reduction of pollution in the environment (Encinas-Romero et al., 2013). This research is unique in the recycling cement bypass dust to be a valuable product named as hydroxyapatite in a Nano scale.

Experimental

Chemicals and Reagents

Waste materials of cement Bypass dust were obtained from Cement factories in Qena governorate. All the reagents as H_3PO_4 acid 85% (NaH_2PO_4), NH_4OH and NaOH were purchased from ALFA and ELNASR Companies. The stock solutions of Fe (III) and Mn (II) were prepared with concentration of 1000 mg/L. The desired pH values of solutions were adjusted by either 0.1 M HCL or 0.1 M NaOH.

Method for fabricated Hydroxyapatite samples

The following steps were employed to produce four Hydroxyapatite samples from Kiln-HA1 to Kiln-HA4, as demonstrated in Fig. 1. Cement bypass dust waste was dissolved in concentrated nitric acid solution with stirring to give clear calcium solution after filtration. Then, 2 ml of H_3PO_4 (85%) was added slowly with

continuously stirring having molar ratio Ca/P of 1.67. After that, the solution of NH_4OH (33%)was added to the above suspension solution until pH value reached 10.The final suspended solution was microwaved for 5 minutes at 170 W for growth of hydroxyapatite crystals. Finally, the Hydroxyapatite was filtered, rinsed in deionized water, and dried overnight at 40°C.

Apparatus

The utilized tools in this research were as following:

- FTIR (Fourier Transform Infrared) measurements (Nicolet) Magna-FTIR – 560 (USA) with KBr technique,
- Powder X-ray Diffraction Analysis (XRD) Brucker Axs-D8- Advance Diffractometer (Belgium) at 2Θ range between 10°–70°.
- TG and DSC device model (50H Shimadzu thermal analyzer, Japan).
- Morphology and elemental analysis SEM & EDX (Model FEI INSPECT S50) operating at 20 kV.
- Surface area measurements BET, total pore volume and pore radius using Automatic ASAP 2010 Micrometrics sorptometer (USA) (Quanatachrome Instruments, version 11.04).
- Iron and manganese ions were determined by multiparameter Bench Photometer (Hanna HI 83208) instruments.

Adsorption Studies

Assessment of the sorption ability of tested hydroxyapatite samples for removal Fe and Mn ions was carried out in batch mode. This is due to its simplicity, consistency, and ease of extrapolation to a larger scale for a practical application. The adsorption parameters were investigated at initial concentration (100–500 ppm), pH (2–10), contact time (1- 120 min), Adsorbent dosage (0.05–0.7 gm. /50 ml) and operating temperature (25–55°C).

The following equations (1,2) were used to calculate the percentage removal efficiency and amount of metal adsorbed (q_e) (El-Nahas, Safaa et al., 2020).

$$\%\ Removal = \frac{(C_o - C_e)}{C_o} \times 100 \quad (1)$$

$$q_e = \frac{(C_o - C_e)}{m} \cdot \frac{V}{1000} \quad (2)$$

Where, the C_o and C_e are the initial metal ion concentration and the final metal ion concentration at equilibrium (mg/L), m is the mass of adsorbent dose (g), V is the volume of the solution (ml).

Determination the Point of Zero Charge (PZC):

0.1 g of dry Hydroxyapatite samples were mixed with 50 ml of NaCl 0.01 M at various pH solutions (2–12), shaken, and maintained at room temperature for 48 hours until equilibrium was reached. The final pH was measured, and the equation ($\Delta pH = pH_i - pH_f$) was used to calculate the Δ pH [15].

Result And Discussion

Characterizations of the synthetic Hydroxyapatite

XR D analysis

The structure of Klin-HA materials was investigated using XRD analysis to detect distinct phases present in the starting powders as well as recognized the chemical composition (El-Nahas, Safaa et al., 2020). Three XRD patterns were showes in Fig. 2 (a,b) for raw cement bypass dust cement and the four prepared hydroxyapatite samples (Kiln-HA), respectively.The data indicated that calcite $CaCO_3$ was the most prevalent component percentage in bypass dust (39.1%), followed by Larnite Ca_2SiO_4 (25.2%) and Al_2O_3 (14.4%), as shown in Fig. 2 (a). Other small components such as SiO_2, Periclase MgO, Fe_2O_3, and CaO were also present, as shown in Table 2, Others identified comparable components in Egyptian cement kiln dust (Salem, W. M. et al., 2015). Furthermore, the XRD pattern revealed that all synthesised hydroxyapatite samples had hexagonal crystal structures, which corresponded to card number COD 9011095 for the pure phase of hydroxyapatite Fig. 2(b) and Table 1. The major diffraction peaks of Kiln-HA were appeared at 2θ = 25.8°, 31.4°, 49.4° and 53.4°(Khawar et al., 2019; Maleki et al., 2019). The crystallite size of the hydroxyapatites studied ranged from 14.85 to 25.72 nm, placing them in the Nano-scale, according to previous research (Abo-El-Enein, 2017).

Table 1
Chemical structure, phases, and the Crystallite size for Hydroxyapatite samples

Sample name	major phase	Chemical structure	JCPDS card	Crystallite size nm
Kiln-HA 1	**Hydroxyapatite**	**$Ca_5HO_{13}P_3$**	**COD 9011092**	**16.43**
Kiln-HA 2	**Hydroxyapatite**	**$Ca_5HO_{13}P_3$**	**COD 9011095**	**25.72**
Kiln-HA 3	**Hydroxyapatite**	**$Ca_5HO_{13}P_3$**	**COD 9011095**	**14.85**
Kiln-HA 4	**Hydroxyapatite**	**$Ca_5HO_{13}P_3$**	**COD 9011095**	**17.12**

Table 2
Chemical composition of Cement by-pass dust

Card	Parameter	% Content
COD 9015835, 9016022	**CaCO3 Calcite**	**39.1%**
COD 1537314	**$K_{1.5}$ $Na_{0.5}$ S**	**11.4%**
COD 9006307	**SiO_2**	**5.9%**
COD 9012790	**Ca_2O_4Si Larnite**	**25.2%**
COD 1200005	**Al_2O_3**	**14.4%**
COD 1528612	**Fe_2O_3**	**1.8%**
COD 1000053	**MgO Periclase**	**1.1%**
COD 1011094	**CaO**	**1.1%**

SEM and EDX analyses

The morphological features of four synthetically Kiln-HA samples are shown in Fig. 3 (a-d). In the case of Kiln-HA1, Kiln-HA2, and Kiln-HA3 samples, the (SEM) photos seemed to be in the shape of a star or coral reefs, while Kiln-HA4 was sheet-like in appearance.Other hydroxyapatite materials have been observed to have a similar morphology (Barakat et al., 2008; Maleki et al., 2019). According to the EDX analysis, the examined materials mostly include P, Ca, O, and H, with trace levels of additional elements including Mg, Fe and Ti Fig. 4 and Table 3show the percentages of elements in the Kiln-HA compound. The obtained ratios matched the XRD patterns and were in good accord with the projected value of 1.67 (Iconaru et al., 2018) .

Table 3
EDX analysis for Hydroxyapatite samples (Kiln-HA1 to Kiln-HA4

samples	Elemental Analysis %									Ca/P
	Na	Mg	Al	Si	P	K	Ca	Ti	Fe	
Kiln-HA 1	**7.40**	**1.00**	**2.47**	**1.04**	**31.63**	**	**52.90**	**	**2.85**	**1.67**
Kiln-HA 2	**8.51**	**0.78**	**2.74**	**	**32.99**	**0.21**	**51.37**	**0.15**	**3.24**	**1.70**
Kiln-HA 3	**4.02**	**1.01**	**2.61**	**0.54**	**34.22**	**0.42**	**54.26**	**0.17**	**2.76**	**1.59**
Kiln-HA 4	**0.42**	**0.90**	**2.39**	**	**36.23**	**0.27**	**56.87**	**	**2.93**	**1.57**

FTIR analysis

Photospectroscopy analysis was employed to validate the functional groups of Kiln-HA.The FT-IR spectrum of the synthesized Kiln-HA nanostructure was seen in Fig. 5. The appeared peak around 3600–3400 cm^{-1} was attributed to the stretching O H.While, peaks displayed around 1600–1500 $cm^{-1}$was recognized to the O Hbending of the surface adsorbed water.The phosphate bands (PO_4^{-3}) for a specific type of apatite were located at 1061-1007cm^{-1},574–533cm^{-1} and 634–607cm^{-1}(Garskaite et al., 2014; Iconaru et al., 2018). The carbonate (CO_3^{2-}) functional group wasappearedat wavenumbers 1405.91cm^{-1} wich was indicatedby thevibration C– O band of (CO_3^{2-}) group. Hydroxyapatite may include some tiny CaO compounds that have the capacity to bind CO2 and form calcium carbonate $CaCO_3$ molecules appeared in FTIR analyses (Garskaite et al., 2014; Popa Cristina Liana et al., 2016) .

Surface area measurements

S_{BET} methods were used to estimate porosity, specific surface area, pore volume, and pore size (El-Nahas, Safaa et al., 2020). The four evaluated hydroxyapatite samples revealed high specific surface area in the order: Kiln-HA3 (161.5 m^2/g) > Kiln-HA1 (130.2 m^2/g) > Kiln-HA2 (81.9 m^2/g) > Kiln-HA4 (54.1 m^2/g) as displayed in Fig. 6 (a, b) and Table 4. The hydroxyapatite samples under investigation have a greater specific surface area than previously published materials (Abo-El-Enein, 2017). At P/P_0, the adsorbed amount reached a limiting value, indicating a type I isotherm with a concave P/P0 axis. The classic I-type denotes the presence of microporous materials (Huang et al., 2019).

Table 4
Surface properties for fabricated hydroxyapatite samples

Sample name	BET square ($m^2.g^{-1}$)	Total pore volume ($cm^3.g^{-1}$)	Aaverage pore radius (A°)
Kiln-HA1	**130.18**	**0.06779**	**10.4**
Kiln-HA2	**81.96**	**0.04111**	**10.03**
Kiln -HA3	**161.49**	**0.08302**	**10.28**
Kiln -HA4	**54.149**	**0.02891**	**10.3**

Thermo-gravimetric analysis

As demonstrated by the TG curves in the heating diagram was in Fig. 7 one stage for the Kiln-HA1 and Kiln-HA2 samples, but was in two stages for the Kiln-HA3 and Kiln-HA4 samples. The total weight losses for tested samples were in the first stage were 10–12%, indicating that all of the samples were thermally stable. The first step of sample weight loss occurred when the temperature was below 100°C, which was ascribed to the release of adsorbed water in the samples. Furthermore, at temperatures below 115°C, water in the channels evaporates, resulting in a one-step approach. The second stage of weight loss appeared solely in Kiln-HA3 and Kiln-HA4 samples around temperature 250°C. Decomposition of nitrates,

acetates, or ammonia in the starting materials may occur at temperatures between 250 and 350°C (Grigoraviciute-Puroniene et al., 2019; Mondal et al., 2016). DTG curves verified the information provided from TG curves. Kiln-HA1 and Kiln-HA2 samples displayed a single DTG peak at 75 ^{o}C and 97 ^{o}C, respectively. While, Kiln-HA3 and Kiln-HA4 samples demonstrated double DTG peaks at (84°C, 249 ^{o}C) and (95 ^{o}C, 252 ^{o}C), respectively. Higher temperatures can produce dehydroxylation in apatite samples, which has been recorded at temperatures beyond 700°C (Garskaite et al., 2014).

The DSC curves revealed that all the peaks below 100 ^{o}C in apatite samples showed endothermic nature owing to evaporated adsorbed water. All hydroxyapatite samples exhibit a substantial wide endothermic peak at 218, 285, 280, and 268°C which are attributable to coordinated water in the lattice. Sharp endothermic peaks at temperatures above 700 ^{o}C were observed due to the decomposition of hydroxyapatite and formation of tri-calcium phosphate (Sava et al., 2015). or formation of $Ca_2P_2O_7$ (Mousa et al., 2013).

Study of Point of Zero Charge (PZC)

For determination of the acidity or basicity of the adsorbent's surface, measurements of the surface pH for tested adsorbent samples were performed (El- Nahas, et al.,2017). Figure 8 depicted the pH_Z of all hydroxyapatite samples, showing that the observed value was around 7.2. The surface will be a positively charged at pH < 7.2 and will be negatively charged with pH > 7.2. A similar approach was observed in other studies (Hokkanen et al., 2018). Cationic species are predicted to commence adsorption at pH values more than 7.2, whereas anionic compounds will be adsorbed at pH levels greater than 7.2 (Ananth et al., 2018; Hokkanen et al., 2018).

Effect of initial pH

One of the most essential topics in terms of practicality was determining the correct pH for optimising the elimination process (Venkatesan et al., 2019). The surface charge of an adsorbent and the degree of ionisation of metals are both affected by the pH of a solution (El Kady et al., 2016). With raising the pH solution, the elimination of Fe (III) and Mn (II) increased dramatically, as seen in Fig. 9(a, b). According to point of zero charge measurements in section (3.2), the cationic metals will be efficiently removed at pH 7.2.The concentration of hydrogen ion (H^+) is large at low pH values, resulting in competition with metal ions over adsorbent sites The Fe (III) and Mn (II) metal ions started to precipitate at pH levels greater than 8. Because effective removals began at pH = 7.2, this was chosen as the optimal pH for for continued adsorption research. Others followed suit (El Kady et al., 2016).

Effect Metal Initial Concentrations

The adsorption mechanism and the number of adsorbent active sites used are both affected by the initial metal ion concentration (Garskaite et al.,2014). Studying the effect of iron and manganese ions concentration on the removal process were employed in the range of 100–500 mg.L^{-1} and the results were domnestrated in Fig. 10 (a,b) According to the findings, when the iron and manganese levels were increased, the removal performance was lowered. As the initial metal ion concentrations increases, the

sorption sites become saturated The existence of a finite number of active sites at a particular dosage of adsorbent might explain the phenomena. Other researchers had the same conclusion (El-Nahas, Safaa et al., 2020).

Effect of Contact Time

It's crucial to know how long water treatment systems take to reach their peak performance. The influence of duration was investigated in this study throughout time intervals ranging from 1 minute to 120 minutes. Initially, the amount of metal ion adsorbed rises quickly until reaching saturation at equilibrium. The metal ions are promptly adsorbed on these sites because there are more adsorption sites accessible at initially, resulting in a rapid spike in the sorption process (Abo-El-Enein, 2017; El Kady et al., 2016). Fe ions were eliminated at a rate of more than 98% in less than one minute, and equilibrium was reached after 20 minutes. In the case of Mn ions, 80% clearance was accomplished in 10 minutes, despite the equilibrium takes longer (120 minutes). The results were illustrated in Fig. 11(a, b). The sluggish adsorption process was related to pore diffusion, once after saturation, both surface and pore binding sites would be occupied, preventing further adsorption (Huang et al., 2019).

Effect of adsorbent dosage

The adsorbent dose is an essential property since the overall surface area has a direct impact on the removal process (Mohandes Salavati-Niasari, 2014). The sorption capacity of Fe and Mn ions were enhanced via increasing amount of adsorbent material. This might be related to the fact that the number of active sites on the surface of adsorbent materials has increased (El-Nahas, Safaa et al., 2020; El Kady et al., 2016) (Huang et al., 2019). Only a minimal dose (0.06 g/L) of Kiln -HA samples was required for more than 96 percent clearance of Fe ions, while sorption of Mn ions required more Kiln-HA samples (at least 1 g/L) to achieve 82 percent removal as illustrated in Fig. 12 (a, b).

Effect of Temperature

The sensitivity of sorption process for changing temperature from 25 to 55°C were demonstrated in Fig. 13 (a, b). The removal of Fe^{3+} and Mn^{2+} augmented significantly with increasing of the temperature. This phenomenon indicating that the adsorption process has the endothermic nature. Various published papers for other hydroxyapatites revealed the endothermic nature of certain metal ion sorption (Gupta et al., 2011) (Qian et al., 2014).

Thermodynamic parameters

The adsorption process is affected by temperature, which causes existing bonds to break and metal cation mobility to rise, leading to the development of new binding adsorption sites (El Kady et al., 2016). The evaluation of thermodynamic parameters is required in order to determine the spontaneity of the adsorption process as well as the feasibility of operation at a certain temperature. The thermodynamic parameters calculated at temperatures of 25, 35, 45, and 55°C were the change in Gibbs free energy (ΔG° in kJ/mol), enthalpy (ΔH° in kJ/mol), and entropy (ΔS° in kJ/mol K). shows the equations that were used to assess these parameters, while the results shown in Table 5 while the results were demonstrated in

Tables 6 and 7 and Fig. 14. At all working temperatures, the hydroxyapatite samples exhibited negative ΔG° values, showing that the adsorption process is feasible and spontaneous. The positive values of ΔH° indicate that the removal of metal ions by apatite materials is an endothermic process. It really revealed a complex interaction between the adsorbate and adsorbents involving numerous processes (as: adsorption & ion exchange) (El Kady et al., 2016; Kim et al., 2020). More negative ΔG° values were obtained as the temperature goes up, indicating that the adsorption process is more favorable at higher temperatures (El-Nahas, Safaa et al., 2020). A positive entropy value suggests an increase in disorder. The entropy change for the system is always positive in a spontaneous process (Abo-El-Enein, 2017).

Table 5 Thermodynamic parameters

Thermodynamic parameters	Equation	Reference
Free energy ΔG° (kJ/mol)	$\Delta G^\circ = RT \ln K_C$ $K_c = C_{ad}/C_e$	
Van't Hoff equation	$\ln Kc = \frac{\Delta S^\circ}{R} - \frac{\Delta H^\circ}{RT}$	(El-Nahas, S. et al., 2020; 2017; 2021)
Enthalpy ΔH° (kJ/mol) Entropy ΔS° (kJ/mol K)	$\Delta G^\circ = \Delta H^\circ - T\Delta S^\circ$	

Table 6
Thermodynamic parameters for adsorption system of Fe ions onto Hydroxyapatite

Sample	ΔH°	ΔS°	Δ G° (kJ/mol)			
	(kJ/mol)	J/mol. K	25°C	35°C	45°C	55°C
Kiln-HA 1	88.06	337.27	-12.45	-15.82	-19.20	-22.57
Kiln-HA 2	55.81	237.52	-14.98	-17.35	-19.73	-22.10
Kiln-HA 3	34.75	143.82	-8.11	-9.54	-10.98	-12.42
Kiln-HA 4	99.77	362.18	-8.16	-11.87	-15.41	-19.03

Table 7
Thermodynamic parameters for adsorption system of Mn ions onto Hydroxyapatite

Sample	ΔH°	ΔS°	Δ G ° (kJ/mol)			
	(kJ/mol)	J/mol. K	25°C	35°C	45°C	55°C
Kiln-HA1	28.70	115.51	-5.72	-6.88	-8.03	-9.19
Kiln-HA2	30.82	120.78	-5.17	-6.38	-7.59	-8.80
Kiln-HA3	5.52	36.15	-5.25	-5.61	-5.97	-6.34
Kiln-HA4	12.89	67.93	-7.35	-8.03	-8.71	-9.39

Equilibrium Studies

Adsorption isotherms are mathematical models that may be used to determine which design is optimal for a certain application. Adsorption isotherms give physicochemical details on how adsorption takes place and how the interaction between the adsorbent surface and the adsorbent happens (El Kady et al., 2016). The three well-known isotherm models parameters used in this research were Langmuir, Freundlich, and Temkin illustrated in Table 8 (Ayawei et al., 2017). The maximal adsorption capacity (q_{max}), which describes monolayer coverage of adsorbate per (g) of adsorbent, is calculated using the Langmuir model.

The plots and values of experimental equilibrium data of Fe (III) and Mn (II) adsorbed on Kiln-HA samples showed higher linearity for all three models (Langmuir, Freundlich, and Temkin), as displayed in Fig. 15 and Tables 9 and 10. That is, all three models are capable of adequately describing the sorption process. The R^2 values of all three models were also relatively comparable to one another, suggesting that Fe(III) and Mn(II) uptake by Kiln-HA samples is intricate and may be explained by several mechanisms (Moreno, et al., 2010). The maximum adsorption capabilities (q_{max}) were found to be between 147 and 175 $mg.g^{-1}$ for Fe (III) whereas varied from 204 to 344 $mg.g^{-1}$to Mn(II).The values of (q_{max}) were greater than those of other hydroxyapatite-adsorbent materials previously published (Ahmed et al., 2021). The R_L value in Langmuir model ranges between 0 and 1 reflected the favorable adsorption process of Fe (III) and Mn (II) ions onto Kiln-HA (Qian et al., 2014). Furthermore, the *n* value for the Freundlich isotherm is larger than unity that indicates the removal of iron and manganese ions is favorable (Darweesh, 2020). Also, high values of K_f indicate high adsorption efficiency for iron and manganese ions by Kiln-HA (El Kady et al., 2016). The binding constants obtained from Temkin isotherm parameters were in range of 67–79 and 21.4–52.4($J.mol^{-1}$) for Fe^{3+} and Mn^{2+}, respectively that showing adsorbents have the higher affinity for binding with the Kiln-HA(Darweesh, 2020). Figures 16 and 17 illustrate the nonlinear patterns of three adsorption models (Langmuir, Freundlich, and Temkin) on hydroxyapatite, which support the linear models' verified findings.

Table 8 Linear and non-linear isotherms equations used in this work

Isotherm models	Linear form	Nonlinear form	Parameter	Reference
Freundlich	$\log q_e = \frac{1}{n}\log Ce + \log K_f$	$q_e = K_f \quad C_e^{\frac{1}{n}}$	q_e adsorption capacity at equilibrium (mg/g) Ce final concentration at equilibrium (mg/l) K_f (l/g) & n Freundlich constants	**(El-Nahas, S. et al., 2017, 2020, 2021)**
Langmuir	$\frac{1}{q_e} = \frac{1}{K_L q_{max}} \cdot \frac{1}{C_e} + \frac{1}{q_{max}}$	$q_e = \frac{q_{max} K_L \quad C_e}{1 + K_L \quad C_e}$	q_{max} (mg/g) Langmuir maximum adsorption capacity K_L Langmuir constant (mg/mg)	
Temkin	$q_e = B\ln A + B\ln C_e$	q_e=B (lnAC_e) B=R_T/b	A(l/mg), b(J/mol) Temkin binding constant at equilibrium B is heat of sorption (J/mol.)	

Table 9
Langmuir, Freundlich and Temkin Isotherm constant Fe ions onto Hydroxyapatite

Sample	Langmuir constants				Freundlich constant			Temkin constant			
	q_{max} (mg. g^{-1})	K_L (mg /L)	R^2	R_L	n	K_f (mg/g)	R^2	b J/mol	B	A	R^2
Kiln-HA 1	159	6.30	0.99	$1.8*10^{-3}$	2.78	117.9	0.98	70	35.4	58.9	0.93
Kiln-HA 2	175	6.33	0.99	$1.8*10^{-3}$	2.90	140.9	0.96	69	36.1	64.7	0.96
Kiln-HA 3	147	8.50	0.98	$1.6*10^{-3}$	2.94	121.3	0.91	79	31.3	69.6	0.99
Kiln-HA 4	172	5.27	0.98	$2.6*10^{-3}$	2.61	107.9	0.97	67	36.9	33.7	0.84

Table 10
Langmuir, Freundlich and Temkin Isotherm constant Mn ions onto Hydroxyapatite

Sample	Langmuir constants				Freundlich constant			Temkin constant			
	q_{max} (mg. g^{-1})	KL (L/mg)	R^2	RL	n	K_f (mg/g)	R2	b J/mol	B	A	R^2
Kiln-HA 1	204	0.042	0.99	0.19	1.94	18.01	0.98	52.36	47.32	0.37	0.99
Kiln-HA 2	344	0.039	0.99	0.20	0.88	3.01	0.94	21.43	115.6	0.16	0.94
Kiln-HA 3	243	0.036	0.99	0.22	1.57	11.59	0.92	38.50	64.34	0.23	0.99
Kiln-HA 4	232	0.069	0.99	0.15	1.63	21.16	0.99	44.71	55.42	0.62	0.96

Kinetic Studies

Kinetic analysis is commonly used to estimate the rate of adsorption and offers valuable insight into the mechanism and rate controlling step of adsorption process (Sultan et al., 2018). Many kinetic models, including pseudo-first-order, pseudo-second order, and intraparticle diffusion, have been employed to study the adsorption process. The linear forms of kinetic models were reported in Table 11 and their plots were shown in Figs. 18 and 19. The sorption process matched the pseudo-second-order kinetic better than the pseudo-first-order kinetic, according to R^2 values as presented in Tables 12 and 13. It's worth noting that the q_e experimental results are virtually identical to those predicted using pseudo-second-order kinetics. Despite the fact that pseudo-second-order kinetics does not fully reflect merely chemical adsorption (El-Nahas, et al., 2020; El Kady et al., 2016). The ion-exchange mechanism at the charged surface can also be articulated by the pseudo-second order model (Plazinski et al., 2009). According to published study, the sorption process suited the pseudo-second-order kinetics model well at lower initial concentrations, whereas the pseudo-first-order kinetics model fit better at greater initial concentrations (Azizian, 2004). Since the plots produced from the intraparticle model (Weber–Morris equation) did not pass through the origin point as illustrated in Fig. 20, the rate-adsorption-controlling step is not solely through the diffusion process (El-Nahas, et al., 2020).

Table 11 Kinetic models used in this work

Kinetic models	Equation	Parameter	Reference
Pseudo-first order	$Log(q_e - q_t) = \log q_e - \frac{K_1}{2.303}t$	q_e and q_t (mg/g) are the adsorbate at equilibrium and at any time t K_1 (min^{-1}) is the pseudo-first order constant.	(El-Nahas, S. et al., 2020;, 2017; 2021)
Pseudo-second order	$\frac{t}{q_t} = \frac{1}{k_2 q_e^2} + \frac{1}{q_e} \cdot t$	K_2 (g/mg. min.) is the pseudo-second order constant	
Intraparticle diffusion	$q_t = k_{ad}\, t^{0.5} + C$	K_{ad} is the intraparticle diffusion rate constant ($mg.g^{-1}.min^{0.5}$) C is the thickness of boundary layer.	

Table 12
Kinetic Studies, pseudo-first, pseudo second and intraparticle diffusion Constant of Fe ions onto Hydroxyapatite

Sample	Pseudo-first order			Pseudo-second order			Intraparticle diffusion			qe
	K_1	q_e	R^2	K_2	q_e	R^2	K_{ad}	R^2	C	(Exp)
Kiln-HA 1	0.013	0.023	0.992	0.762	45.0	0.999	0.002	0.977	44.96	44.99
Kiln-HA 2	0.008	0.12	0.992	1.57	43.59	0.999	0.015	0.974	43.47	43.59
Kiln-HA 3	0.072	0.09	0.899	0.797	43.90	0.999	0.088	0.750	42.92	43.89
Kiln-HA 4	0.062	0.34	0.881	0.614	43.07	0.999	0.032	0.884	42.73	43.06

Table 13
Kinetic Studies, pseudo-first, pseudo second and intraparticle diffusion Constant of Mn ions onto Hydroxyapatite

Sample	Pseudo-first order			Pseudo-second order			Intraparticle diffusion			q_e
	K_1	q_e	R^2	K_2	q_e	R^2	K_{ad}	R^2	C	(Exp)
Kiln-HA 1	0.014	15.81	0.927	0.003	47.62	0.999	0.363	0.810	34.47	47.25
Kiln-HA 2	0.001	4.80	0.753	0.069	44.84	0.999	0.162	0.876	42.58	48.50
Kiln-HA 3	0.002	5.18	0.990	0.022	44.19	0.999	0.367	0.982	39.97	45.75
Kiln-HA 4	0.009	5.27	0.943	0.019	46.34	0.999	0.312	0.90	42.38	48.0

Mechanism for removing of Fe and Mn ions on Kiln-HA surface

According to the findings of this study, The removal of Fe and Mn ions via Klin-HA samples was explained by two pathways; an ion exchange mechanism and an adsorption process.XRD analysis indicated the

formation of substituted metal-hydroxyapatite Ca_5-xMx$(PO_4)_3$(OH) as seen in Fig. 20 (a,b). The major diffraction peaks for Fe-HA detected at 2-theta were 25.7, 31.6, and 28.5 for loaded Fe^{2+} ions, and peak strength dropped as other diffraction peaks faded away (Huang, et al., 2019). The substituted Mn-hydroxyapatite $Ca_2Mn_3(PO_4)_3$(OH) were identified by XRD analysis (COD 2236693) after adsorption process As a result, the ion exchange mechanism appears to have played a role in the elimination process. Adsorption on HA surfaces is the first mechanism, followed by an ion exchange interaction between metal ions adsorbed and Ca^{2+} ions on HA surfaces, according to previous researchers (Moreno et al., 2010).

The electronegativity of Fe and Mn ions in aqueous solution is greater than that of the Ca ion in apatite, which might explain how hydroxyapatite samples can remove metal ions from water via the replacement process (Abdulaziz and Faid, 2013). Furthermore, Ca^{2+} sites have a larger ionic radius (0.99 Å), but Fe^{3+} (0.64 Å) and Mn^{2+} (0.80 Å) have a smaller ionic radius which appears to have an appreciable influence (bin Jusoh, A., et al.2005; Horta, M., et al, 2019; Sirait, M., et al, 2020). It has been demonstrated that calcium phosphate acts not only as a source of adsorption centers but also enables ion-exchange process (Moreno et al., 2010). The replacement process or ion exchange appeared according to the following. (3):

$$Ca_5(PO_4)_3(OH) + X\ (Fe^{3+} \text{or } Mn^{2+}) \rightarrow Ca_{5-x}\ (Fe^{3+} \text{or} Mn^{2+})_x(PO_4)_3(OH) + X\ (Fe^{3+} \text{or} Mn^{2+}) \ldots (3)$$

Where (x) refer to the substituted calcium ions by iron or manganese ions. The hydroxyapatite lattice is very flexible, allowing for effects and vacancies in either cationic or anionic locations (Encinas-Romero et al., 2013).

Metals removal in binary and tertiary system

In most water sources, iron and manganese ions coexist with other cations. We tested mixture of varied proportions of (Fe^{3+}: Mn^{2+}) solutions as (1:1), (2:1), and (1:2) with a total concentration of 100 mg/L. That explore the completion process of eliminating both iron and manganese ions from aqueous solutions via the active site of Kiln-HA samples. As illustrated in Fig. 21(a,b,c), the findings demonstrated that removing Fe (III) from aqueous solutions took priority over removing Mn (II) in all three cases studied. That can be explained as the Fe^{3+}ions have a stronger electronegativity and a smaller ionic radius than Mn^{2+} which explains its selectivity (Samuelsson et al., 2007). Moreover, variations in hydration energy and hydrated ionic radii across metal ions also contributed to this selectivity (Pan et al., 2016). The competitive elimination of Fe $^{3+}$ in the mixed metal ions combination (Fe/Mn/ Cu) showed a similar trend to the binary (Fe^{3+}/Mn^{2+}) solution.Metal ions were eliminated in the following order: Fe^{3+}> Cu^{2+}> Mn^{2+} as dommnestrated in Table 14. For other cations, additional researcher revealed a similar tendency (Pan et al., 2016). In this research, the manufactured Kiln-HA had a greater adsorption capability to different metal ions, indicating that hydroxyapatite is a promising adsorbent to remediate real wastewater

Table 14
mixture of metal ions (Fe^{3+}, Mn^{2+} and Cu^{2+}) affect the removal efficiency

Sample name	Fe^{3+} Removal%	Mn^{2+} Removal%	Cu^{2+} Removal%
KilnHA1	**99.9%**	**87.4%**	**99.5%**
KilnHA2	**99.8%**	**89.5%**	**99.4%**
KilnHA3	**99.9%**	**77.0%**	**95.4%**
KilnHA4	**99.8%**	**79.0%**	**97.8%**

Continuous Reusability of Nano-hydroxyapatite

When an adsorbent can be reused numerous times with acceptable efficiency, the cost to set up an adsorption process is minimized (Khawar et al., 2019). Continuous sorbent reusability enhances system performance and lowering operational costs over time. The adsorption experiment was carried out three cycles continuously without regeneration and their results represented in Fig. 22 (a, b). Ability of Kiln-HA samples to remove Fe and Mn ions were up to 90% for both cations in the first cycle. However, after 3 cycles the adsorption ability had dropped to 20% without regeneration. It can be concluded that the synthetic adsorbents of Kiln-HA are effective and may be utilized several times with good adsorption capacity.

Comparative Study with previous studies

A comparison of different adsorbents' adsorption capabilities against synthesized hydroxyapatite were displayed in Table 15. Kiln-HA' samples had a greater maximum adsorption capacity, ranging from 147 to 175 mg/g for Fe^{3+} and from 204 to 344 mg/g for Mn^{2+}.The recycling of cement bypass to useable hydroxyapatite materials exhibited superior iron and manganese ion elimination efficiency from aqueous solution than other published papers. The hydroxyapatite materials employed in this work are efficient adsorbents with a lot of potential for extracting iron and manganese ions from water at extremely high concentrations (100–1000 ppm).

Table 15

Comparative Study of tested Hydroxyapatite with published materials for removal of Fe^{+3} and Mn^{+2} ions

Materials	Max adsorption capacity (mg/g)	Initial conditions (ppm)	%Removal efficiency	References
Natural Apatite	0.174 mmol/g for Fe^{3+}	Conc. Fe 200 ppm	90% for Fe +3	(Qian et al., 2014)
Magnetotactic bacteria	47.86 mg/g for Fe^{2+} 15.26 mg/g for Mn^{2+}	Conc. Fe 3ppm Mn 8 ppm	48% Fe 15% Mn	(Diaz-Alarcon et al., 2019)
AC from Local Argo-Residues	10.64 mg/g for Fe^{3+} 6.66 mg/g for Mn^{2+}	Conc. Fe & Mn 5ppm	12% Fe 13% Mn	(A. Akl, 2013)
Cow Bone Charcoal	31.43 mg/g for Fe^{2+} 29.56 mg/g for Mn^{2+}	Conc. Fe & Mn 20 ppm	30% Fe &Mn	(Moreno et al., 2010)
Modified Nano-Hydroxyapatite -MgO	0.603 for Fe^{2+} mg/g	Conc. Fe 2 ppm	60% for Fe +3	(Ayash et al., 2019)
Granular activated carbon	3.60 mg/g for Fe^{2+} 2.54 mg/g for Mn^{2+}	Not included	Not included	(Bin Jusoh et al., 2005)
Nano-hydroxyapatite	55.2 mmol/g for Fe^{2+}	Conc. Fe 100 ppm	95% for Fe	(Abo-El-Enein S., 2017)
white rice husk ash	15.2 mg/g for Mn^{2+}	Conc. Mn 20 ppm	15% for Mn	(Tavlieva et al., 2015)
Iron and manganese-coated pumice	Not included	Conc. Fe 15 ppm Mn 5 ppm	84% Fe 72% Mn	(Indah et al., 2017)
Zeolite Y	31.45 mg/g for Fe^{2+} 18.02 mg/g for Mn^{2+}	Conc. Fe 1.15 ppm Mn 1.61 ppm	96% Fe 83% Mn	(Kwakye-Awuah et al., 2019)

Materials	Max adsorption capacity (mg/g)	Initial conditions (ppm)	%Removal efficiency	References
microporous chitosan/polyethylene glycol	71.4 for Fe^{2+} 18.5 mg/g for Mn^{2+}	Conc. Fe & Mn 2 ppm	Not included	(Reiad et al., 2012)
superparamagnetic Nano-hydroxyapatite	0.54 mg/g for Fe^{2+} 0.61 mg/g for Mn^{2+}	Conc. Fe & Mn 50 ppm	85% Fe &Mn	(El Kady et al., 2016)
Removal of Iron and Manganese by precipitation	Not included	Conc. Fe 0.1 ppm Mn 0.05 ppm	92% Fe 96% Mn	(Salem, M. et al., 2012)
Apatite IITM	126 mg/g for Fe^{2+} 124 mg/g for Mn^{2+}	Conc. Fe &Mn 75 ppm	98% Fe 96% Mn	(Oliva et al., 2010)
Modified Hydroxyapatite	0.389 mg/g for Fe^{3+}	Conc. Fe 2 ppm	50% for Fe^{3+}	(El nsar et al., 2017)
Nano hydroxyapatite Kiln-HA1 Kiln-HA2 Kiln-HA3 Kiln-HA4	159 mg/g for Fe^{3+} 175 mg/g for Fe^{3+} 147 mg/g for Fe^{3+} 172 mg/g for Fe^{3+}	204 mg/g for Mn^{2+} 344 mg/g for Mn^{2+} 243 mg/g for Mn^{2+} 232 mg/g for Mn^{2+}	99% Fe 96% Mn	This study

Cost assessment of synthesized Nano- hydroxyapatite

If the source of Ca ions was affordable and free, the cost of manufacturing hydroxyapatite would be reduced. Waste cement bypass dust is a rich source of both $CaCO_3$ and CaO which can be utilized in the hydroxyapatite production process. As a result, the initial components are cheap, enabling the implementation of a low-cost method. Costs connected with the processing of Kiln-HA samples were largely driven by energy consumed. Making 100 g of hydroxyapatite from recycled cement bypass dust

cost were around 184 EGP/100g (9.32 € /100g). Table 16 displayed the price for manufacturing100 g of hydroxyapatite from different calcium sources. The hydroxyapatite powders from cement bypass were lower than those published by Sigma Company. The manufacturing of powder nano- HA price (surface area > 80 m^2/g) published by Sigma-Aldrich company were 462 € which equal 9162 (EGP) (Aldrich, 2022).

Table 16
The total cost of the materials that were tested

hydroxyapatite Samples	Cost/100g by (EGP) chemicals - electricity	Price of HA (€/100 g)	References
HA-Cl	258 £	13.02 €	(Safaa El-Nahas, 2022)
HA-NO_3	386 £	19.47 €	
HA-OH	263 £	13.27 €	
HA-AC	278 £	14.02 €	
Kiln-HA	184 £	9.32 €	This study
HA® Sigma-Aldrich	9162 £	462 €	(Aldrich, 2022)

Field Study in Real Water Samples

Two groundwater well samples were taken that had already been polluted with iron and manganese ions at quantities of 2.46 and 0.11 mg/L, respectively. For polluted water with Fe and Mn ions, all of the examined hydroxyapatite samples had a clearance efficiency of 99.9%.The results reveal that hydroxyapatite materials may remove Fe and Mn ions from groundwater wells even when other cations (such as Ca, Mg, and Al) or anions (e.g.: NO_3, NO_2, SO_4, Cl, SiO_4) are present. A variety of goals, such as the accessibility of clean drinking water via cheap adsorbent materials as well as the sustainable management of our waste resources, were achieved in this study.

Conclusion

This research is the first of its type in terms of recycling cement bypass dust via turning it into a usable product called hydroxyapatite in Nano scale. The nano powder hydroxyapatite exhibited good physical properties, including crystallite sizes less than 50 nm. Moreover, the surface area of these synthetic materials was large, with a BET ranging from 65 to 161.m^2g^{-1}.

- The prepared Kiln-HA from cement bypass dust exhibited 99% removal for iron and manganese ions from various water sources.
- The removal efficiency was in a short period of time (15 minutes) with minimal dosage (2 $g.L^{-1}$).

- The hydroxyapatite samples can be used for three continuous cycles, exhibiting a strong capacity for Fe^{3+} and Mn^{2+}removal over a wide pH range.
- The removal of Fe and Mn ions fit well the isotherm models of Langmuir, Freundlich, and Temkin fit well.
- Pseudo-second-order model and intraparticle diffusion model fit the removal process.
- All the hydroxyapatite samples used had a positive ΔH° value indication the endothermic nature.
- The hydroxyapatite sample can be utilized in a single, binary, or multi metal ions system, with up to 85% metal removal effectiveness.
- According to employing cement bypass waste as a source of calcium, the total cost of synthesizing 100 g of hydroxyapatite is only around 184 EGP/100g (9.3 € /100g).
- Findings of this study aimed to fulfill a number of SDGs, including availability of safe drinking water (goal 6), as well as sustainable management and efficient use of natural resources (goal 12).

Declarations

Author Contributions: Conceptualization, supervision, writing— review and editing, validation, S. El- Nahas; A.E. Mohamed; M.S. Abd El-Sadek ; methodology; formal analysis; data curation, R.R. Ahmed. All authors have read and agreed to the published version of the manuscript

Funding: No funding.

Institutional Review Board Statement: Not applicable.

Informed Consent Statement: Not applicable.

Data Availability Statement: Did not report any data

Acknowledgments: The authors extend their appreciation to the Deanship of Faculty of science, South Valley University, Egypt for facilitating the experimental section of this work.

Conflicts of Interest: The authors declare no conflict of interest and that they have no known competing financial interests or personal relationships that could have appeared to influence the work reported in this paper.

References

1. Akl A, M.2013."*Removal of Iron and Manganese in Water Samples Using Activated Carbon Derived from Local Agro-Residues*".Journal of Chemical Engineering & Process Technology, *04*04. doi: 10.4172/2157-7048.1000154
2. Abdel Maksoud MIA, Elgarahy AM, Farrell C, Al-Muhtaseb AaH, Rooney, DWandOsman, A.I.2020."*Insight on water remediation application using magnetic nanomaterials and biosorbents.*

".Coordination Chemistry Reviews, *403*. doi: 10.1016/j.ccr.2019.213096

3. Abdulaziz AM, Faid AM2013."*Evaluation of the groundwater resources potential of Siwa Oasis using three-dimensional multilayer groundwater flow model, Mersa Matruh Governorate, Egypt*".Arabian Journal of Geosciences, *8*2,659–675. doi: 10.1007/s12517-013-1199-4
4. Abo-El-Enein SE-B, Elkorashey H, Sery A (2017) Synthesis and characterization of nano-hydroxyapatite and its application in removal of Fe and Al ions from their aqueous solutions. Nat Sci 15. doi:10.7537/marsnsj150317.14
5. Ahmad A, van der Wal A, Bhattacharya P, Genuchten CM2019."*Characteristics of Fe and Mn bearing precipitates generated by Fe(II) and Mn(II) co-oxidation with O2, MnO4 and HOCl in the presence of groundwater ions*".Water Res, *161*,505–516. doi: 10.1016/j.watres.2019.06.036
6. Ahmed AM, Ayad MI, Eledkawy MA, Darweesh MA 2021."*Removal of iron, zinc, and nickel-ions using nano bentonite and its applications on power station wastewater*".*Heliyon, 7*2, e06315. doi:10.1016/j.heliyon.2021.e06315
7. Aldrich.2022." *Hydroxyapatite*". Hydroxyapatite. Retrieved from https://www.sigmaaldrich.com/EG/en/substance/hydroxyapatite5023112167747
8. ALOthman ZA (2012) "A Review: Fundamental Aspects of Silicate Mesoporous Materials" Materials 512:2874–2902. doi:10.3390/ma5122874
9. Ananth KP, Sun J, Bai J2018."*An Innovative Approach to Manganese-Substituted Hydroxyapatite Coating on Zinc Oxide(-)Coated 316L SS for Implant Application*".Int J Mol Sci, *19*8,2340. doi: 10.3390/ijms19082340
10. Ayash, MA.-E.-A.A., Elnasr, TAS, Soliman MH2019."*Removing Iron Ions Contaminants from Groundwater Using Modified Nano-Hydroxyapatite by Nano Manganese Oxide*".Journal of Water Resource and Protection, *11*06,789–809. doi: 10.4236/jwarp.2019.116048
11. Ayawei N, Ebelegi, AN.andWankasi, D2017."*Modelling and Interpretation of Adsorption Isotherms*".Journal of Chemistry, *2017*,1–11. doi:Artn 303981710.1155/2017/3039817.
12. Azizian S2004."*Kinetic models of sorption: a theoretical analysis*".J Colloid Interface Sci, *276*1,47–52. doi: 10.1016/j.jcis.2004.03.048
13. Barakat NAM, Khalil KA, Sheikh FA, Omran AM, Gaihre B, Khil, SMandKim, HY2008."*Physiochemical characterizations of hydroxyapatite extracted from bovine bones by three different methods: Extraction of biologically desirable HAp*".Materials Science & Engineering C-Biomimetic and Supramolecular Systems, *28*8,1381–1387. doi: 10.1016/j.msec.2008.03.003
14. bin Jusoh A, Cheng WH, Low WM, Nora'aini AandMegat, Mohd Noor MJ2005."*Study on the removal of iron and manganese in groundwater by granular activated carbon*".*Desalination, 182*1-3,347–353. doi: 10.1016/j.desal.2005.03.022
15. Czapik P, Zapala-Slaweta J, Owsiak, ZandStepien(2019) P.2020."*Hydration of cement by-pass dust*".*Construction and Building Materials, 231*, 117139. doi:ARTN11713910.1016/j.conbuildmat.117139

16. Darweesh H(2020) "*Hazardous-Effects-of-Electrostatic-Precipitator-Cement-Kiln-Bypass-Dust-Waste-on-both-Environment-and-Public-Human-Health*". *In: Malik Badshah, editor. Prime Archives in Biosciences. Hyderabad,India: Vide Leaf.* 2020. i>www.videleaf.com.
17. Diaz-Alarcon JA, Alfonso-Perez MP, Vergara-Gomez I, Diaz-Lagos, MandMartinez-Ovalle, SA2019."*Removal of iron and manganese in groundwater through magnetotactic bacteria*".J Environ Manage, *249*,109381. doi: 10.1016/j.jenvman.2019.109381
18. El-Nahas S, Osman AI, Arafat AS, Al-Muhtaseb, AaHandSalman, HM2020."*Facile and affordable synthetic route of nano powder zeolite and its application in fast softening of water hardness*".Journal of Water Process Engineering, *33*. doi: 10.1016/j.jwpe.2019.101104
19. El-Nahas S, Salman, HandSeleem, W.2017."*A New and Successful Utilization of Egyptalum Company Solid Waste in Adsorptive Removal of Nitrates from Water Supplies*".International Research Journal of Pure and Applied Chemistry, *15*3,1–17. doi: 10.9734/irjpac/2017/38221
20. El-Nahas S, Salman, HMandSaber, AM2021."*Production of low-price carbon for removal of aluminium ions in potable water*".Journal of Environmental Engineering and Science, *16*3,145–164. doi: 10.1680/jenes.20.00055
21. El kady M, Shokry, HandHamad, H2016."*Effect of superparamagnetic nanoparticles on the physicochemical properties of nano hydroxyapatite for groundwater treatment: adsorption mechanism of Fe(ii) and Mn(ii)*".RSC Advances, *6*85,82244–82259. doi: 10.1039/c6ra14497g
22. Elnsar TAS, Soliman, MHandAyash, MA.-E.-A.A.J.C.o.A.M.2017."*Modified hydroxyapatite adsorbent for removal of iron dissolved in*water wells in Sohag, Egypt". 21,1–13
23. Encinas-Romero MA, Peralta-Haley J, Valenzuela-García, JLandCastillón-Barraza, FF2013."*Synthesis and Structural Characterization of Hydroxyapatite-Wollastonite Biocomposites, Produced by an Alternative Sol-Gel Route*".Journal of Biomaterials and Nanobiotechnology, *04*04,327–333. doi: 10.4236/jbnb.2013.44041
24. Garskaite E, Gross KA, Yang SW, Yang TCK, Yang, JCandKareiva, A.2014."*Effect of processing conditions on the crystallinity and structure of carbonated calcium hydroxyapatite (CHAp)*".*Crystengcomm, 16*19, 3950–3959. doi:10.1039/c4ce00119b
25. Georgieva VG, Tavlieva MP, Genieva, SDandVlaev, LT2015."*Adsorption kinetics of Cr(VI) ions from aqueous solutions onto black rice husk ash*".Journal of Molecular Liquids, *208*,219–226. doi: 10.1016/j.molliq.2015.04.047
26. Ghorab HY, Mounir A, Ghabrial N, Rizk M, Badawi, SandKhafaga, M.2004."*Resuse of Cement Kiln Bypass Dust in the Manufacture of Ordinary Portland Cement*".Polymer-Plastics Technology and Engineering, *43*6,1723–1734. doi: 10.1081/ppt-200040077
27. Grigoraviciute-Puroniene I, Zarkov A, Tsuru K, Ishikawa, KandKareiva, A.2019."*A novel synthetic approach for the calcium hydroxyapatite from the food products*".Journal of Sol-Gel Science and Technology, *91*1,63–71. doi: 10.1007/s10971-019-05020-4
28. Gupta N, Kushwaha, AKandChattopadhyaya, MC2011."*Adsorptive removal of Pb2+, Co2 + and Ni2 + by hydroxyapatite/chitosan composite from aqueous solution*".Journal of the Taiwan Institute of

Chemical Engineers. doi: 10.1016/j.jtice.2011.07.009

29. Han SX, Ning ZW, Chen, KandZheng, J.2017."*Preparation and tribological properties of Fe-hydroxyapatite bioceramics*".Biosurface and Biotribology, *3*2,75–81. doi: 10.1016/j.bsbt.2017.07.001
30. Hokkanen S, Bhatnagar A, Srivastava V, Suorsa, VandSillanpaa, M2018."*Removal of Cd(2+), Ni(2+) and PO4(3-) from aqueous solution by hydroxyapatite-bentonite clay-nanocellulose composite*".Int J Biol Macromol, *118*Pt A,903–912. doi: 10.1016/j.ijbiomac.2018.06.095
31. Horta M, Aguilar M, Moura F, Campos J, Ramos, VandQuizunda, A.2019."*Synthesis and characterization of green nanohydroxyapatite from hen eggshell by precipitation method*".*Materials Today-Proceedings, 14*, 716–721. doi:DOI 10.1016/j.matpr.2019.02.011
32. Huang LH, Sun, XYandOuyang, JM2019."*Shape-dependent toxicity and mineralization of hydroxyapatite nanoparticles in A7R5 aortic smooth muscle cells*".Sci Rep, *9*1,18979. doi: 10.1038/s41598-019-55428-9
33. Ibrahim M, Labaki M, Giraudon, JMandLamonier, JF2020."*Hydroxyapatite, a multifunctional material for air, water and soil pollution control: A review*".J Hazard Mater, *383*,121139. doi: 10.1016/j.jhazmat.2019.121139
34. Iconaru SL, Motelica-Heino M, Guegan R, Beuran M, Costescu, AandPredoi, D.2018."*Adsorption of Pb (II) Ions onto Hydroxyapatite Nanopowders in Aqueous Solutions*".Materials (Basel), *11*11,2204. doi: 10.3390/ma11112204
35. Indah S (2017) Evaluation of iron and manganese-coated pumice from Sungai Pasak, West Sumatera, Indonesia for the removal of Fe (II) and Mn (II) from aqueous solutions. Green Urbanism (Gu) 37:556–563. doi:10.1016/j.proenv.2017.03.042
36. Khawar A, Aslam Z, Zahir A, Akbar I (2019) Synthesis of Femur extracted hydroxyapatite reinforced nanocomposite and its application for Pb(II) ions abatement from aqueous phase. Int J Biol Macromol 122:667–676. doi:10.1016/j.ijbiomac.2018.10.223
37. Kim M, Choong CE, Hyun S, Park, CMandLee, G.2020."*Mechanism of simultaneous removal of aluminum and fluoride from aqueous solution by La/Mg/Si-activated carbon*".*Chemosphere, 253*, 126580. doi:10.1016/j.chemosphere.2020.126580
38. Kwakye-Awuah B, Sefa-Ntiri B, Von-Kiti E, Nkrumah, IandWilliams, C.2019."*Adsorptive Removal of Iron and Manganese from Groundwater Samples in Ghana by Zeolite Y Synthesized from Bauxite and Kaolin*".*Water, 11*9. doi:ARTN 191210.3390/w11091912
39. Maleki B, Chahkandi M, Tayebee R, Kahrobaei S, Alinezhad H (2019) ."*Synthesis and characterization of nanocrystalline hydroxyapatite and its catalytic behavior towards synthesis of 3,4-disubstituted isoxazole-5(4H)-ones in water*". Appl Organomet Chem 3310:e5118. doi:10.1002/aoc.5118
40. Mohandes, FandSalavati-Niasari, M.2014."*In vitro comparative study of pure hydroxyapatite nanorods and novel polyethylene glycol/graphene oxide/hydroxyapatite nanocomposite*".Journal of Nanoparticle Research, *16*9. doi: 10.1007/s11051-014-2604-y
41. Mondal S, Dey AandPal, U.2016."*Low temperature wet-chemical synthesis of spherical hydroxyapatite nanoparticles and their in situ cytotoxicity study*".Advances in nano research, *4*4,295–307. doi:

10.12989/anr.2016.4.4.295

42. Moreno JC, Gomez, RandGiraldo, L.2010."*Removal of Mn, Fe, Ni and Cu Ions from Wastewater Using*Cow Bone Charcoal".Materials, *3*1,452–466. doi: 10.3390/ma3010452
43. Mousa, SandHanna, A.2013."*Synthesis of nano-crystalline hydroxyapatite and ammonium sulfate from phosphogypsum waste*".Materials Research Bulletin, *48*2,823–828. doi: 10.1016/j.materresbull.2012.11.067
44. Oliva J, De Pablo J, Cortina JL, Cama, JandAyora, C.2010."*The use of Apatite II to remove divalent metal ions zinc(II), lead(II), manganese(II) and iron(II) from water in passive treatment systems: column experiments*".J Hazard Mater, *184*1-3,364–374. doi: 10.1016/j.jhazmat.2010.08.045
45. Pan Y, Liu Z, Wang W, Peng C, Shi, KandJi, X.2016."*Highly efficient macroporous adsorbents for toxic metal ions in water systems based on polyvinyl alcohol–formaldehyde sponges*".Journal of Materials Chemistry A, *47*,2537–2549. doi: 10.1039/c5ta09295g
46. Peethamparan S, Olek JandLovell, J.2008."*Influence of chemical and physical characteristics of cement kiln dusts (CKDs) on their hydration behavior and potential suitability for soil stabilization*".Cement and Concrete Research, *38*6,803–815. doi: 10.1016/j.cemconres.2008.01.011
47. Peters CS1998."*Investigative and management techniques for cement kiln dust and pulp and paper process wastes*".Environmental Progress, *17*3,142–147. doi:DOI 10.1002/ep.670170311
48. Plazinski W, Rudzinski, WandPlazinska, A.2009."*Theoretical models of sorption kinetics including a surface reaction mechanism: a review*".Adv Colloid Interface Sci, *152*1-2,2–13. doi: 10.1016/j.cis.2009.07.009
49. Liana PC, Albu M, Bartha C, Costescu A, Luculescu C, Trusca RandS, A.2016."*Structural Characterization And Optical Properties Of Hydroxyapatite/Collagen Matrix*".Romanian Reports in Physics, *68*3,1149–1158
50. Qian G, Li M, Wang F (2014) ."*Removal of Fe3 + from Aqueous Solution by Natural Apatite*". J Surf Eng Mater Adv Technol 0401:14–20. doi:10.4236/jsemat.2014.41003
51. Reiad NA, Salam A, Abadir OE, andHarraz EF, F.A.2012."*Adsorptive removal of iron and manganese ions from aqueous solutions with microporous chitosan/polyethylene glycol blend membrane*".J Environ Sci (China), *24*8,1425–1432. doi: 10.1016/s1001-0742(11)60954-6
52. Roth DB2015."*Cement Kiln Dust and By-Pass Dust from Cement Kilns*".Amec Foster Wheeler Environment & Infrastructure UK Limited. doi: 10.24425/gsm.2019.128524
53. Abo-El-Enein SA, El-korashy HAEb R. M., A. A. Sery.2017."*Synthesis and characterization of nano-hydroxyapatite and its application in removal of Fe and Al ions from their aqueous solutions*". doi: 10.7537/marsnsj150317.14
54. El–Nahas S, M.a.R AE(2022) R.A. *Structural and Morphological Features of Hydroxyapatite Nanoparticles from Different Calcium Resources*
55. Salem MG, El-Awady MdH, Amin E2012."*Enhanced Removal of Dissolved Iron and Manganese from Nonconventional Water Resources in Delta District*,Egypt".Energy Procedia, *18*,983–993. doi: 10.1016/j.egypro.2012.05.113

56. Salem WM, Sayed WF, Halawy SA, Elamary RB2015."*Physicochemical and microbiological characterization of cement kiln dust for potential reuse in wastewater treatment*".Ecotoxicol Environ Saf, *119*,155–161. doi: 10.1016/j.ecoenv.2015.05.012
57. Samuelsson P, Halvarsson B, Carlsson B2007."*Cost-efficient operation of a denitrifying activated sludge process*".Water Res, *41*11,2325–2332. doi: 10.1016/j.watres.2006.10.031
58. Sava BA, Tardei C, Simonescu CM, Boroica L, Melinescu, A.2015."*Hydroxyapatite nanopowders obtained by sol-gel method, synthesis and properties*".Optoelectronics and Advanced Materials-Rapid Communications, *9*11 – 12,1415–1424
59. Sultan ME, Abo-El-Enein SA, Sayed AZ, EL-Sokkary, TMandHammad, HA2018."*Incorporation of cement bypass flue dust in fly ash and blast furnace slag-based geopolymer*".Case Studies in Construction Materials, *8*,315–322. doi: 10.1016/j.cscm.2018.02.009
60. Tavlieva MP, Genieva SD, Georgieva VG, Vlaev LT (2015) Thermodynamics and kinetics of the removal of manganese(II) ions from aqueous solutions by white rice husk ash. J Mol Liq 211:938–947. doi:10.1016/j.molliq.2015.08.015
61. Venkatesan S, Hassan Mu, Ryu HJ2019."*Adsorption and immobilization of radioactive ionic-corrosion-products using magnetic hydroxyapatite and cold-sintering for nuclear waste management applications*".Journal of Nuclear Materials, *514*,40–49. doi: 10.1016/j.jnucmat.2018.11.026
62. Zeb K, Ali Y, Khan MW2019."*Factors influencing environment and human health by cement industry: Pakistan a case in point*".Management of Environmental Quality, *30*4,751–767. doi: 10.1108/Meq-06-2018-0112
63. Huang LH, Sun, XYandOuyang, JM2019."*Shape-dependent toxicity and mineralization of hydroxyapatite nanoparticles in A7R5 aortic smooth muscle cells*".Sci Rep, *9*1,18979. doi: 10.1038/s41598-019-55428-9

Figures

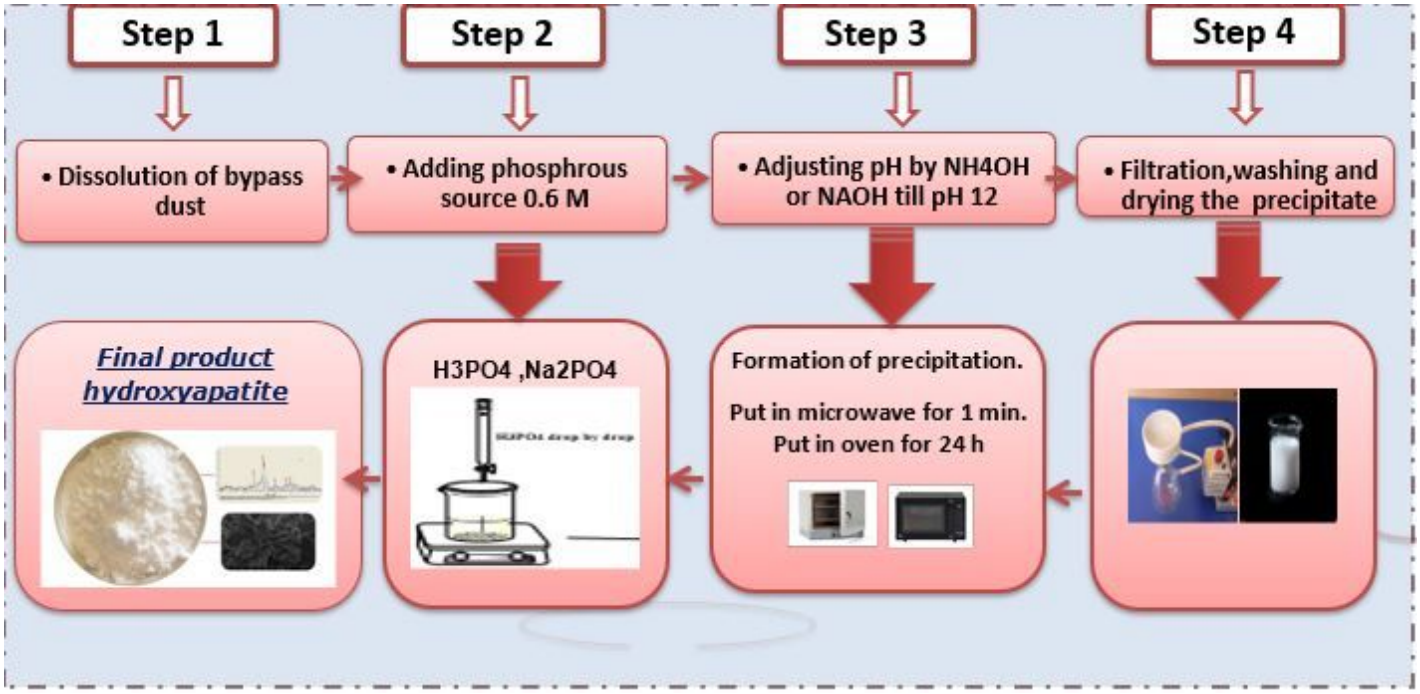

Figure 1

Method for preparation of hydroxyapatite samples (Kiln-HA1-KilnHA4)

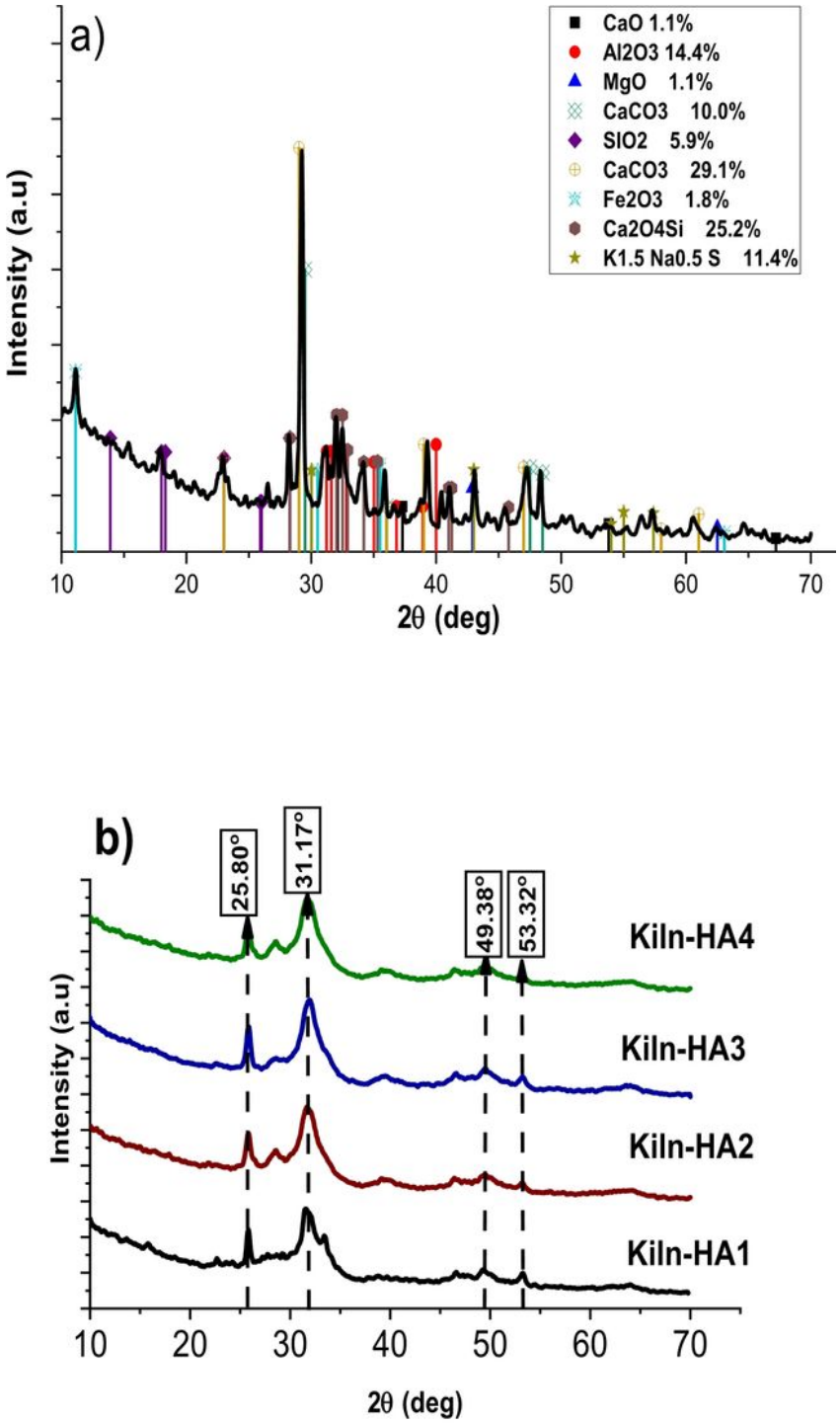

Figure 2

XRD pattern for: a) Cement bypass dust waste b) fabricated hydroxyapatite samples (Kiln-HA1 to Kiln-HA4)

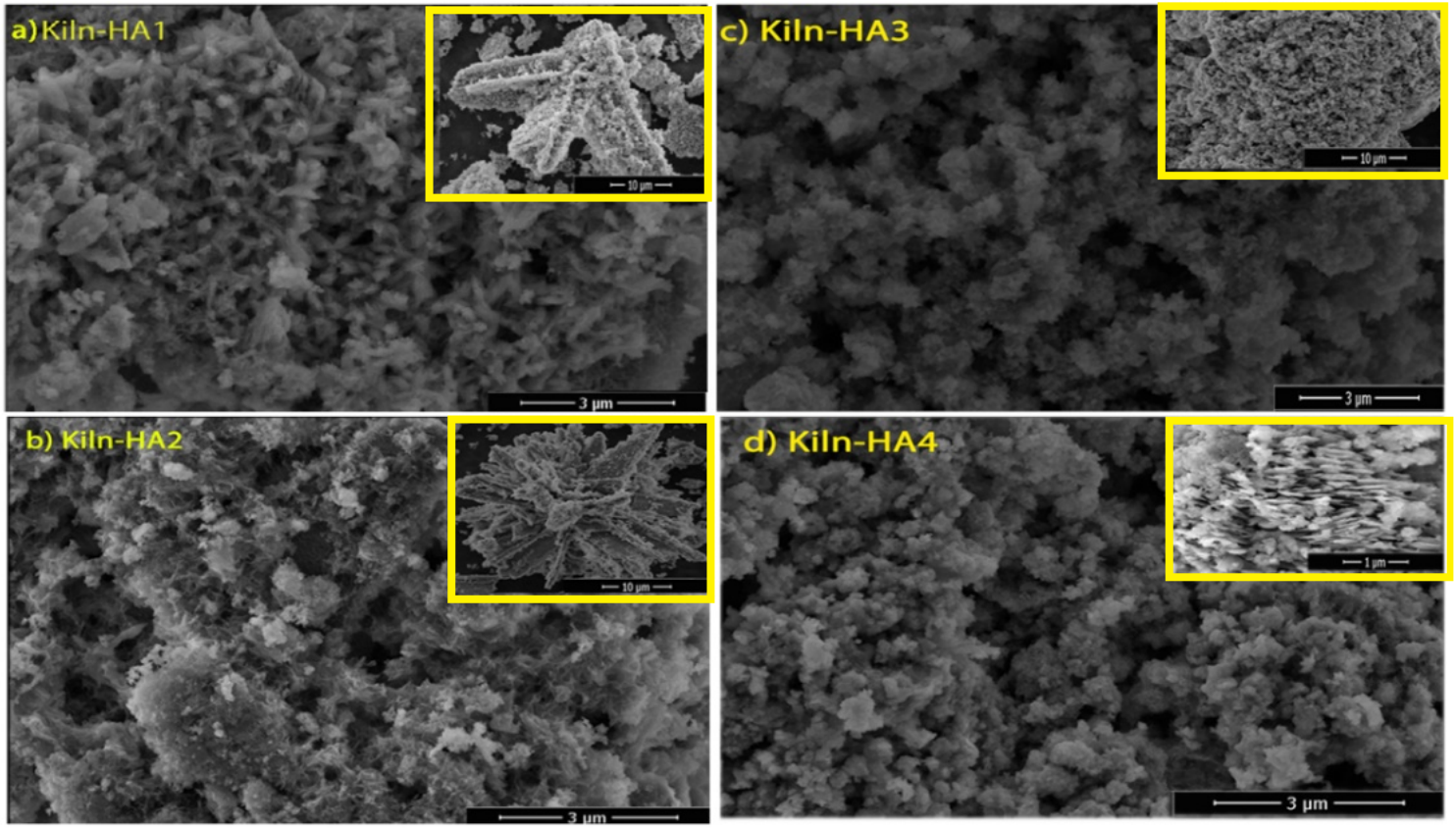

Figure 3

SEM morphology for synthetic hydroxyapatite samples (Kiln-HA1 to Kiln-HA4)

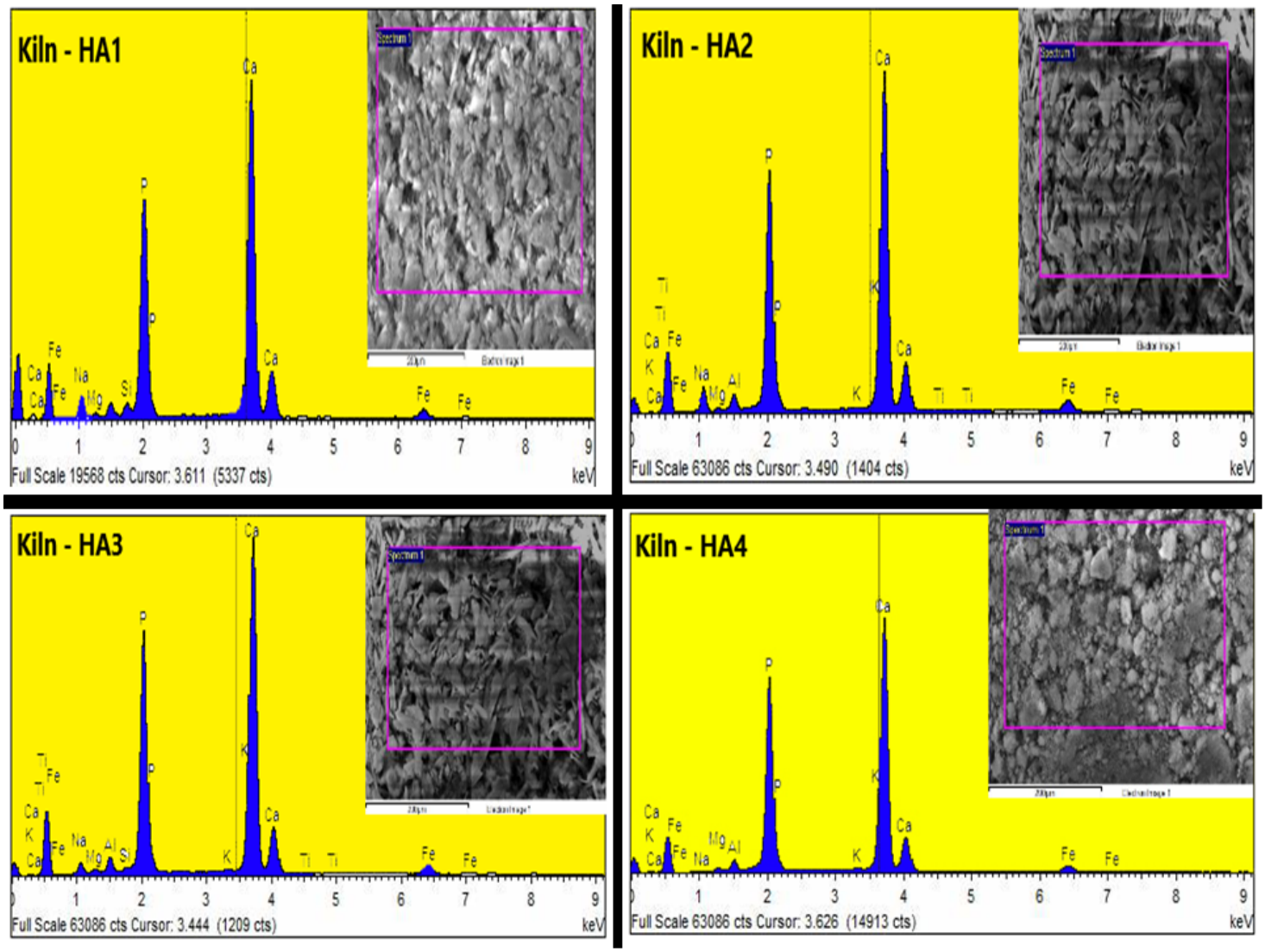

Figure 4

EDX data for synthesized hydroxyapatite samples (Kiln-HA1 to Kiln-HA4)

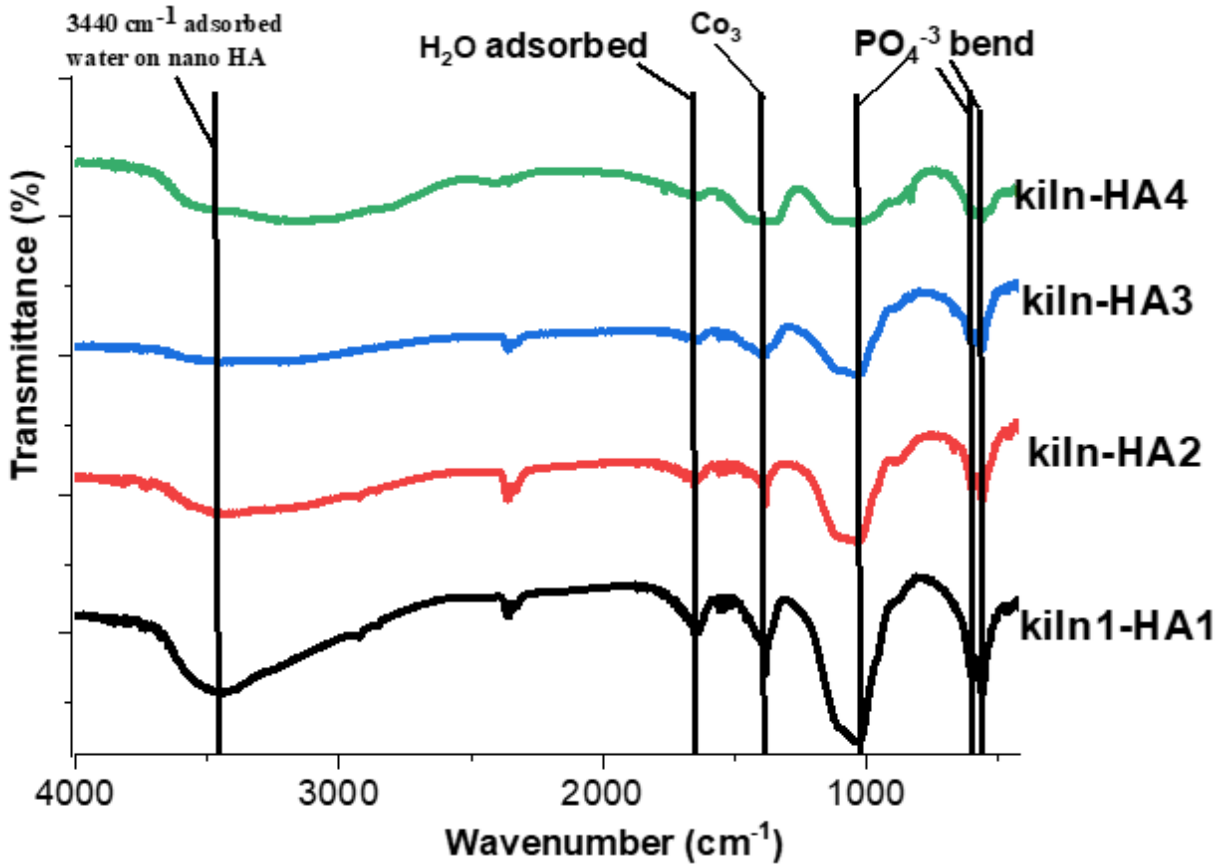

Figure 5

FTIR spectra for fabricated hydroxyapatite samples (Kiln-HA1 to Kiln-HA4)

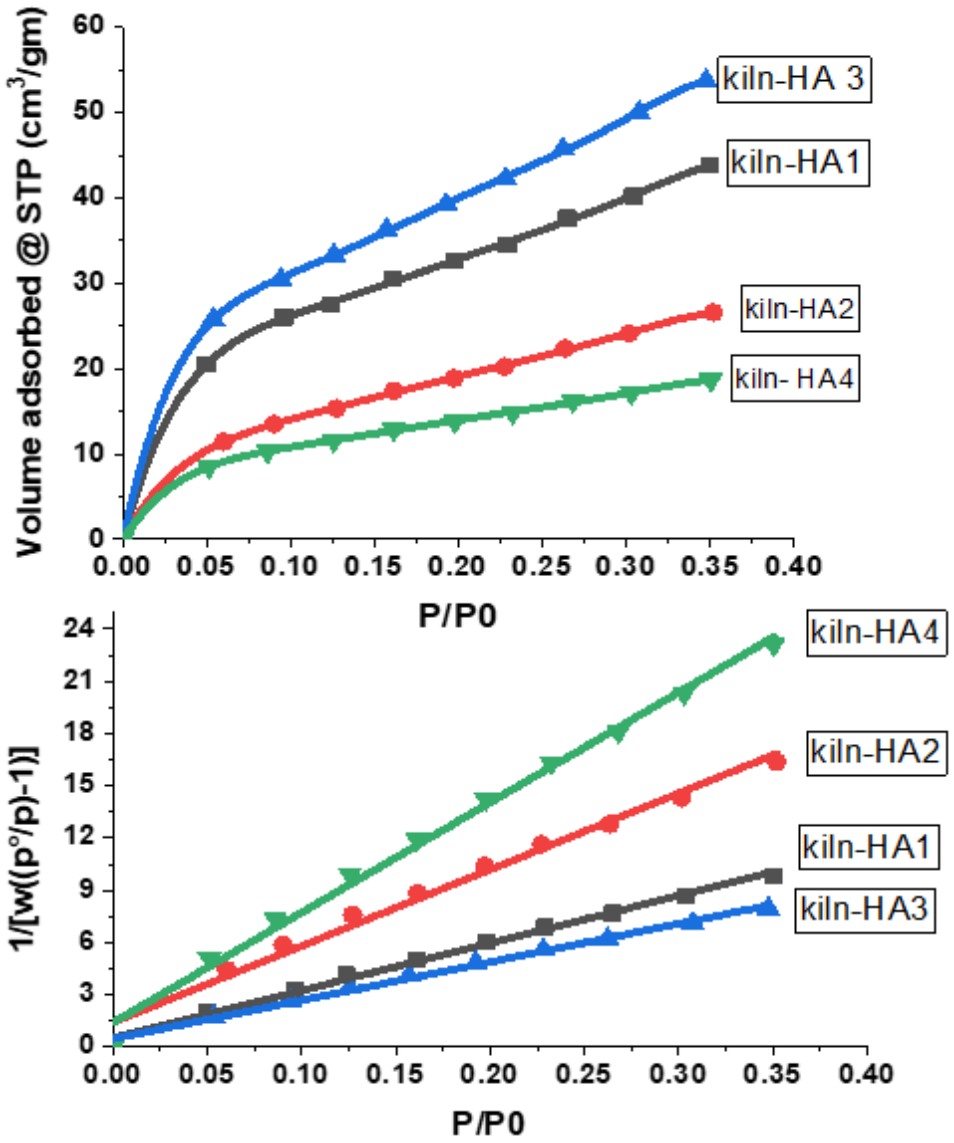

Figure 6

Texture properties for hydroxyapatite samples a) surface areas by BET theory b) N2 adsorption isotherm

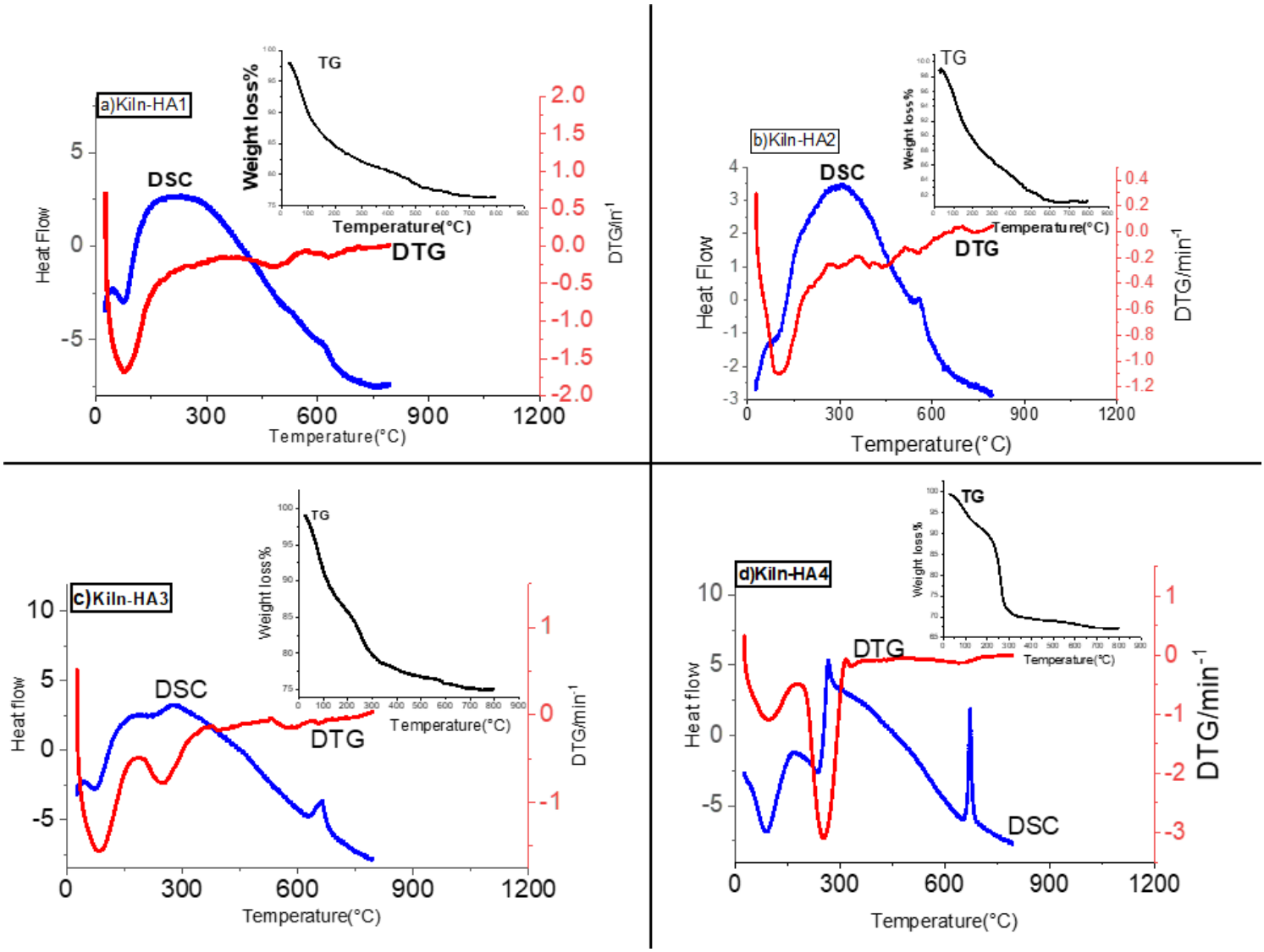

Figure 7

TG, DTG and DSC curves for hydroxyapatite samples (Kiln-HA1 to Kiln-HA4)

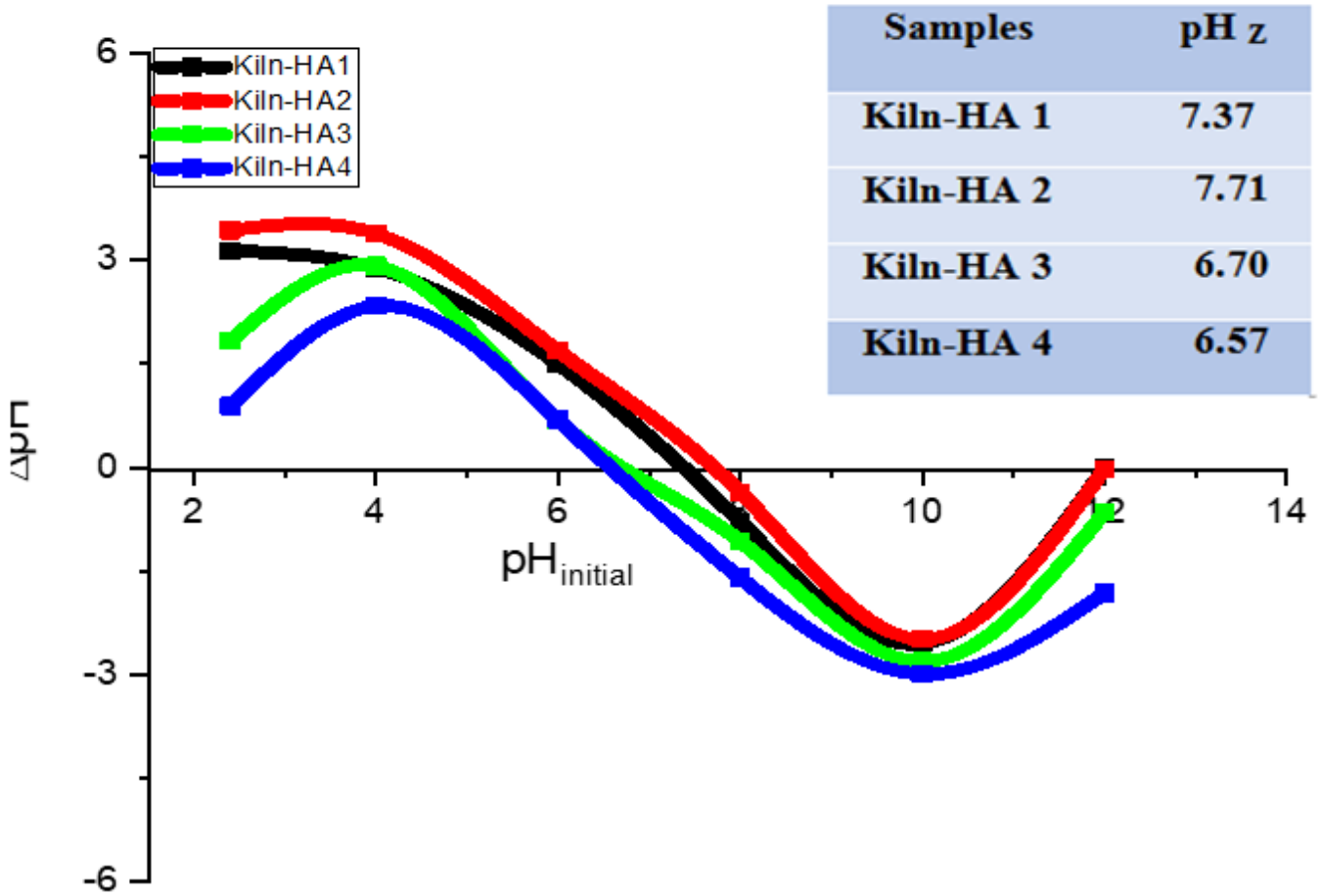

Samples	pH z
Kiln-HA 1	7.37
Kiln-HA 2	7.71
Kiln-HA 3	6.70
Kiln-HA 4	6.57

Figure 8

The point of zero charge (pHpzc) for samples (Kiln-HA1 to Kiln-HA4)

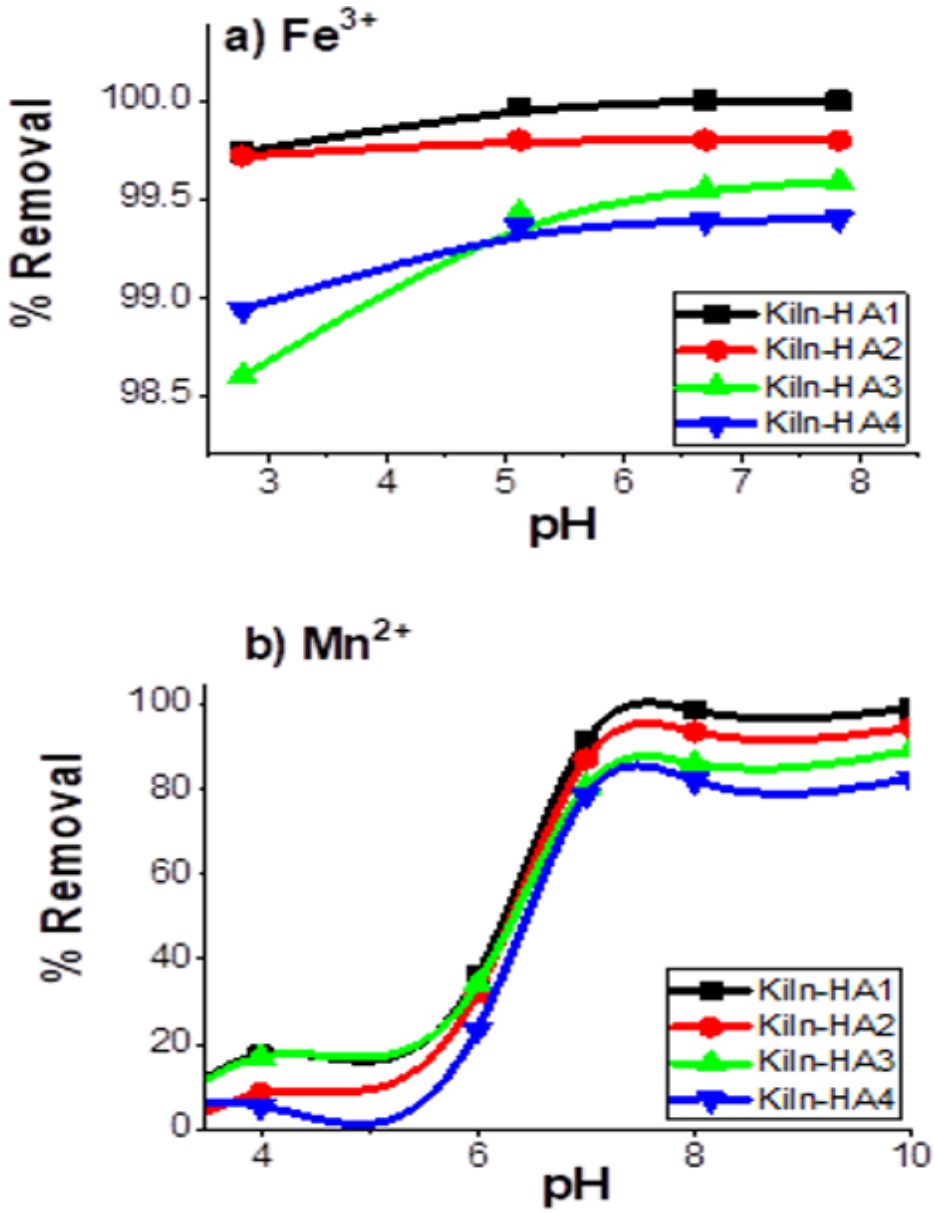

Figure 9

Effect of pH on iron and manganese ions removal using Kiln-HA

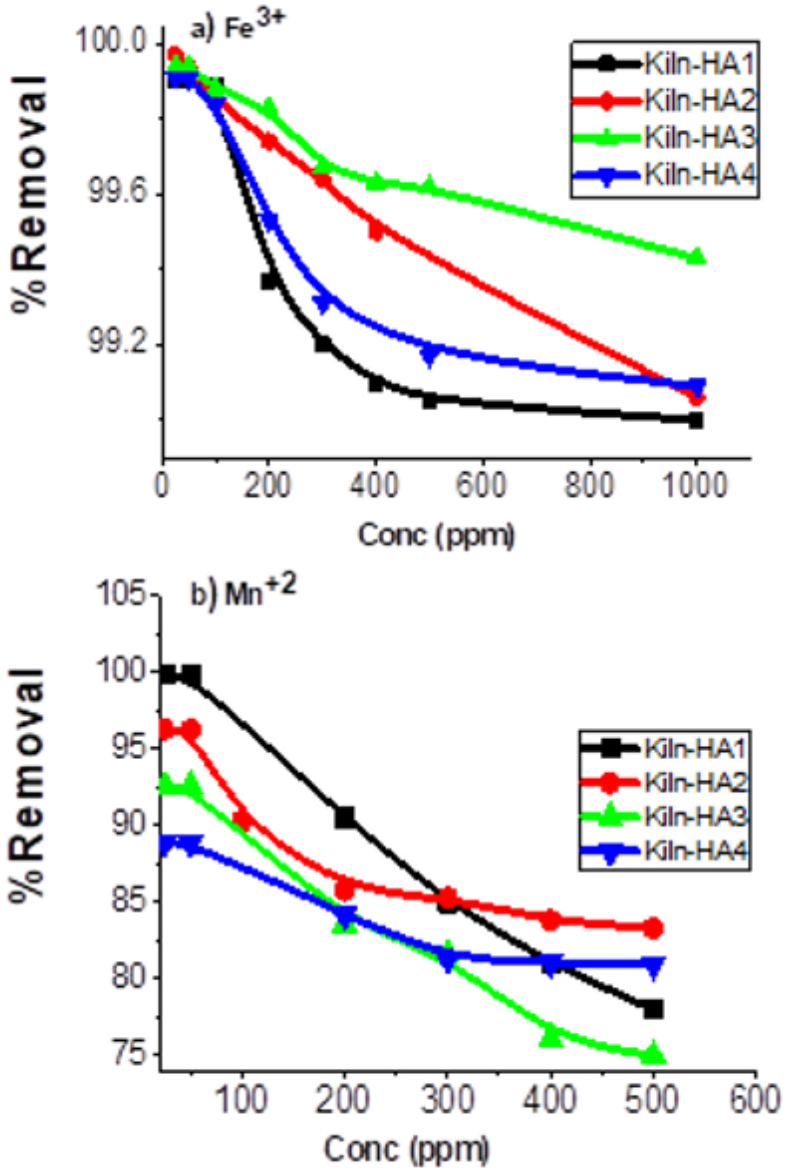

Figure 10

Effect of initial concentration of iron and manganese ions removal using Kiln-HA

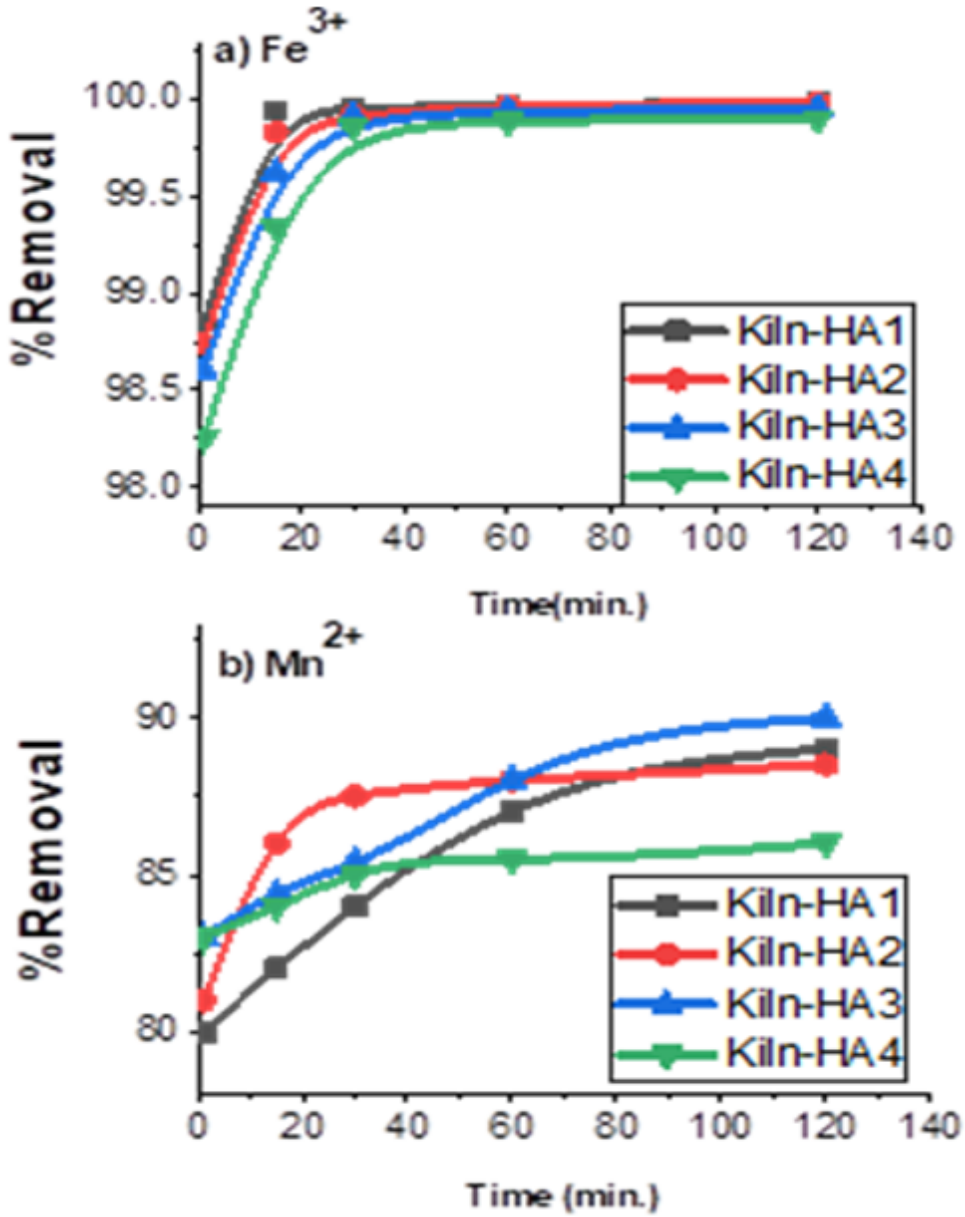

Figure 11

Effect of contact time on iron and manganese ions removal using Kiln-HA

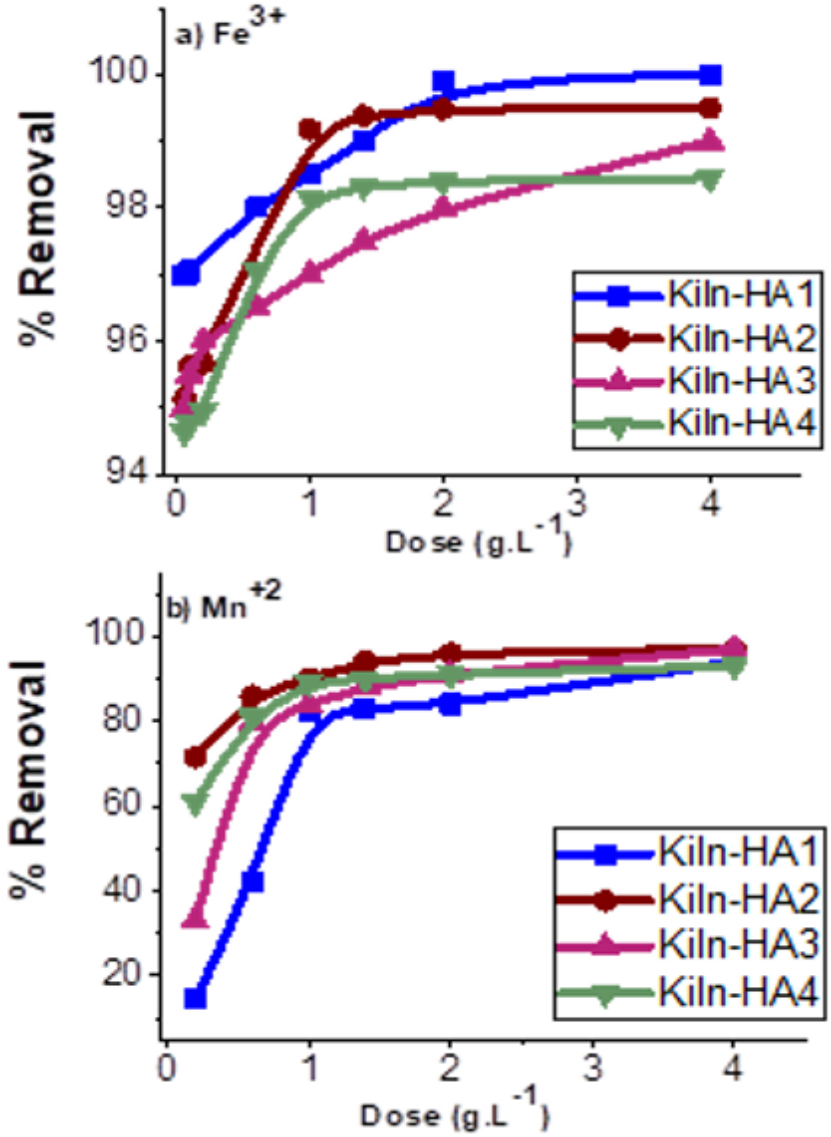

Figure 12

Effect of adsorbent dose on iron and manganese ions removal using Kiln-HA

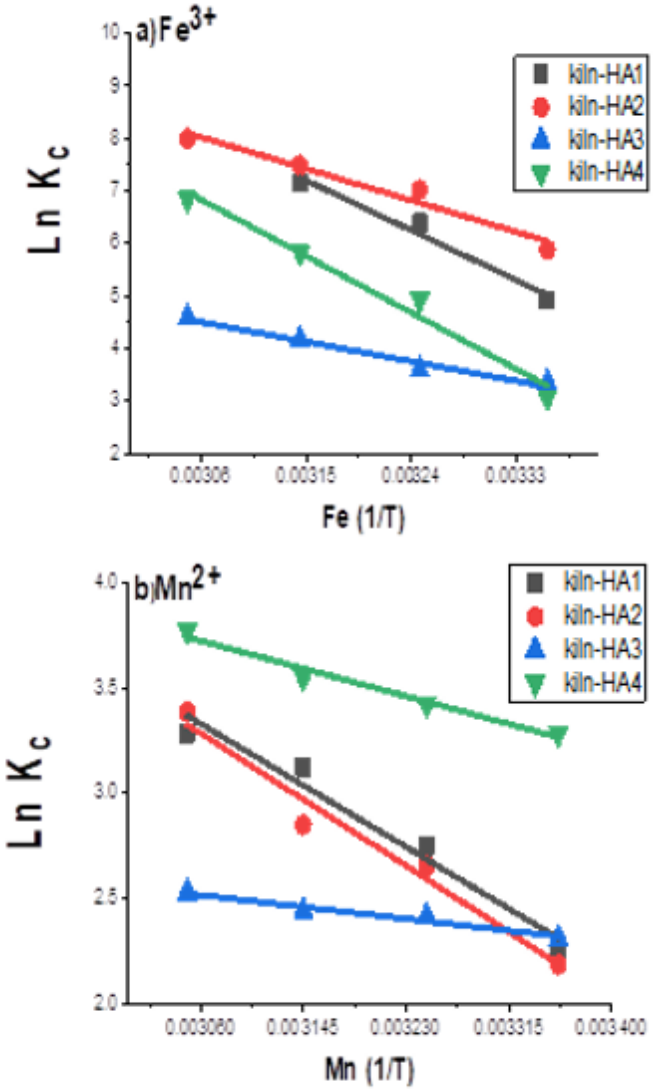

Figure 13

Effect of adsorbent Temperature on iron and manganese ions removal using HAp

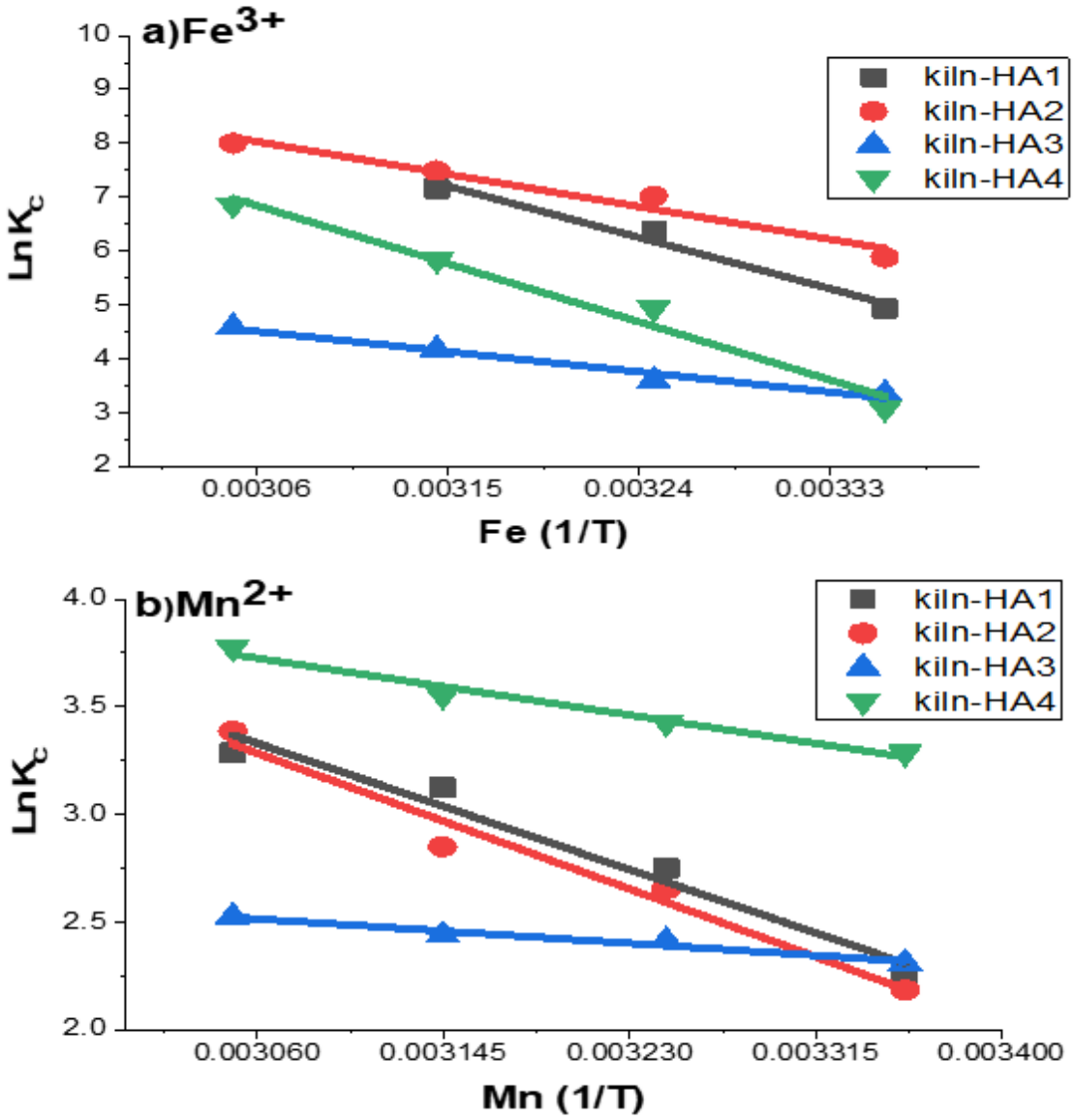

Figure 14

Plot of ln (Kc) versus 1/T for hydroxyapatite samples (Kiln-HA1 to Kiln-HA4).

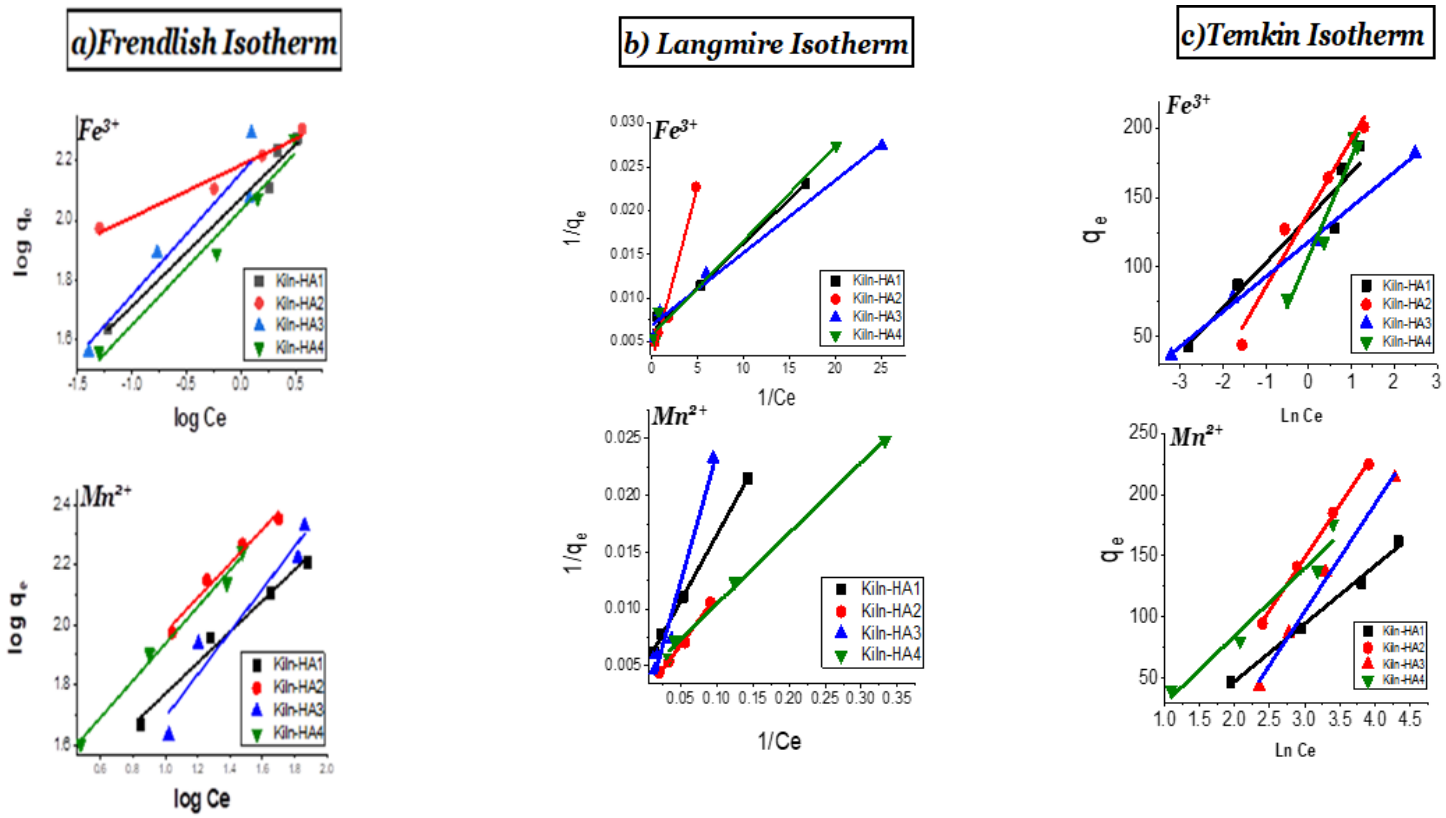

Figure 15

Linear form of a) Freundlich, b) Langmuir and c) Temkin Isotherm of Fe and Mn ions onto Hydroxyapatite

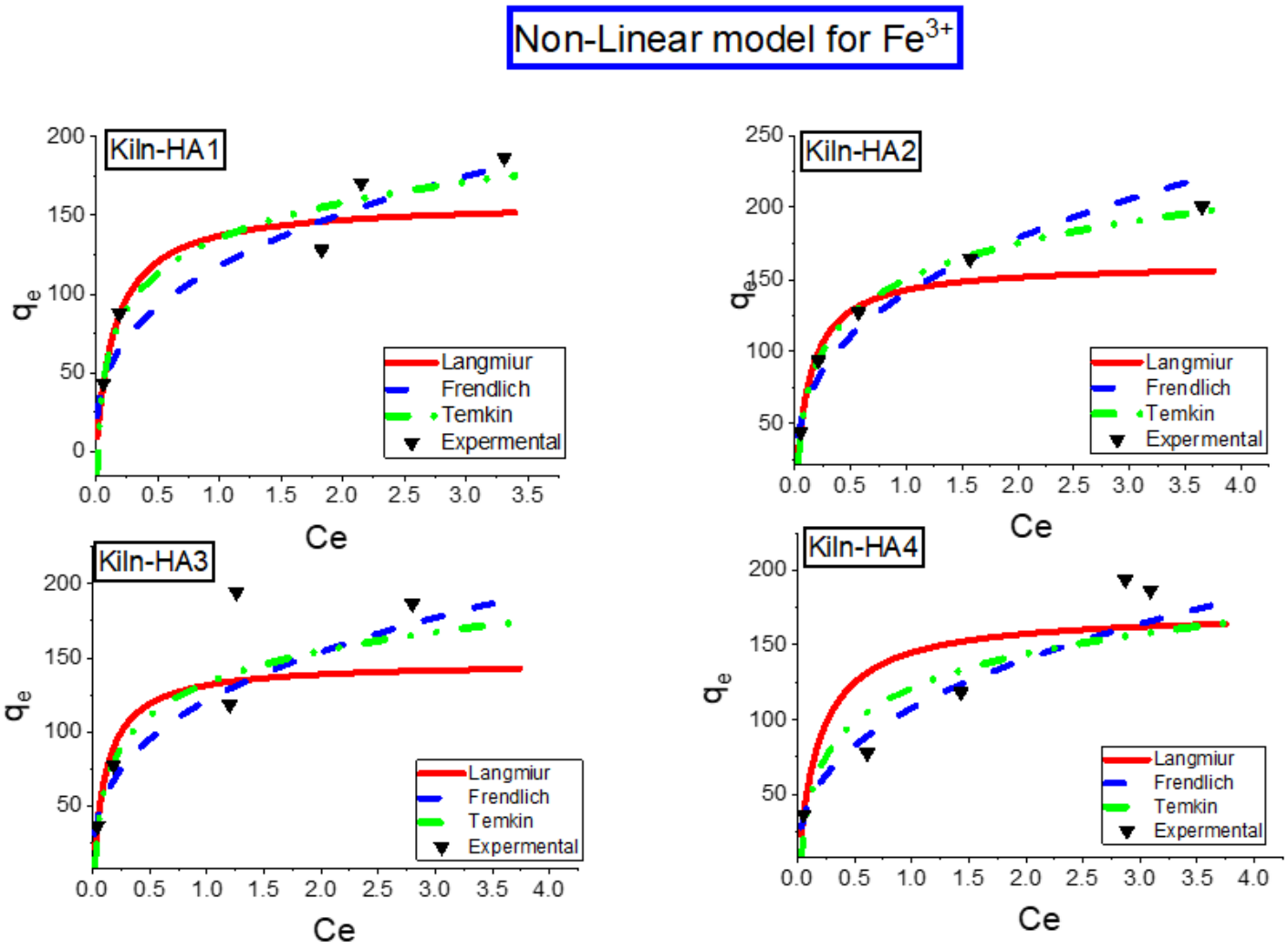

Figure 16

Non-linear form of Freundlich, Langmuir and Temkin Isotherm on adsorption of Fe (III) on sample (Kiln-HA1), B) sample (Kiln-HA2), C) sample (Kiln-HA3), D) sample (Kiln-HA4).

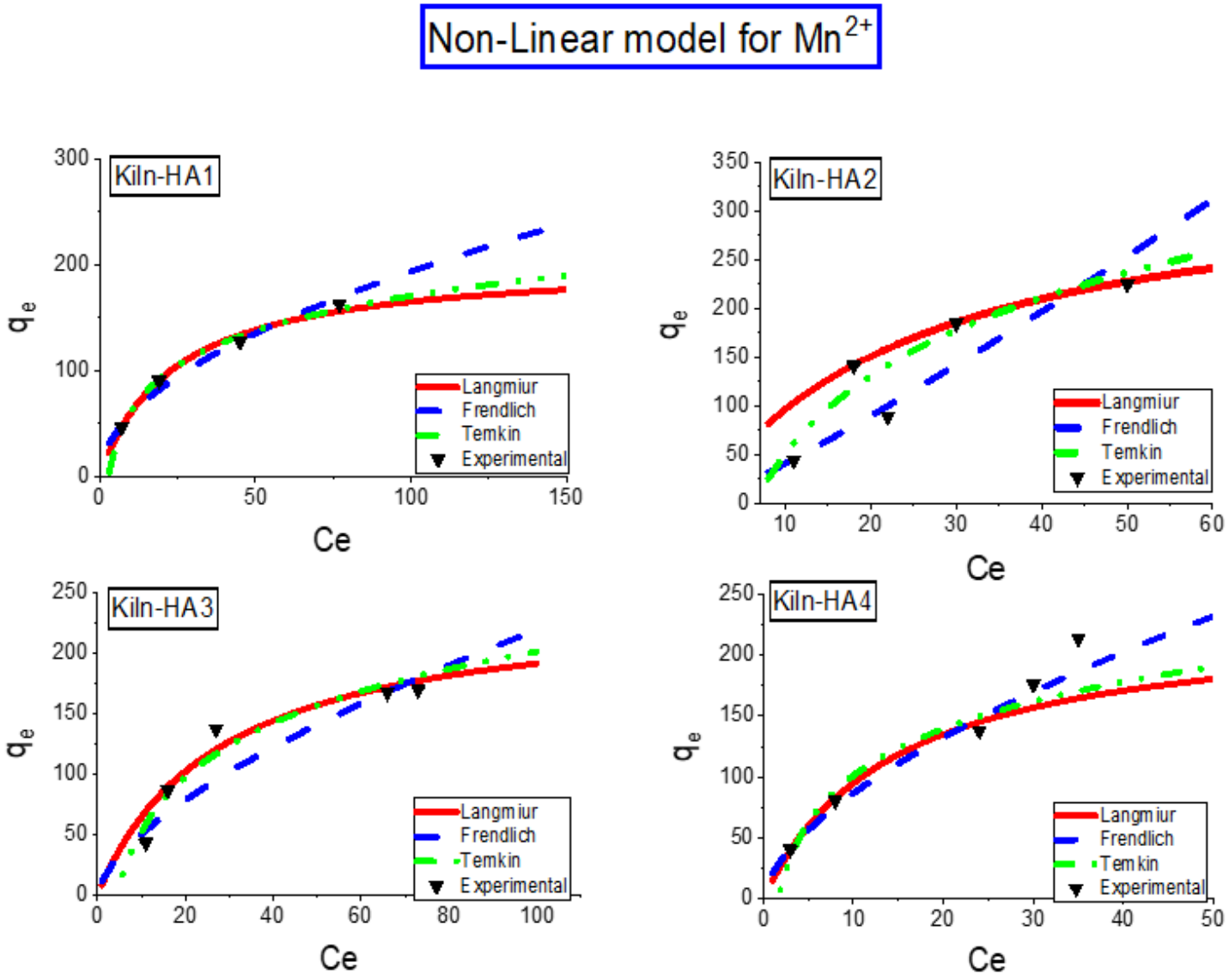

Figure 17

Non-linear form of Freundlich, Langmuir and Temkin Isotherm on adsorption of Mn (II) on sample (Kiln-HA1), B) sample (Kiln-HA2), C) sample (Kiln-HA3), D) sample (Kiln-HA4).

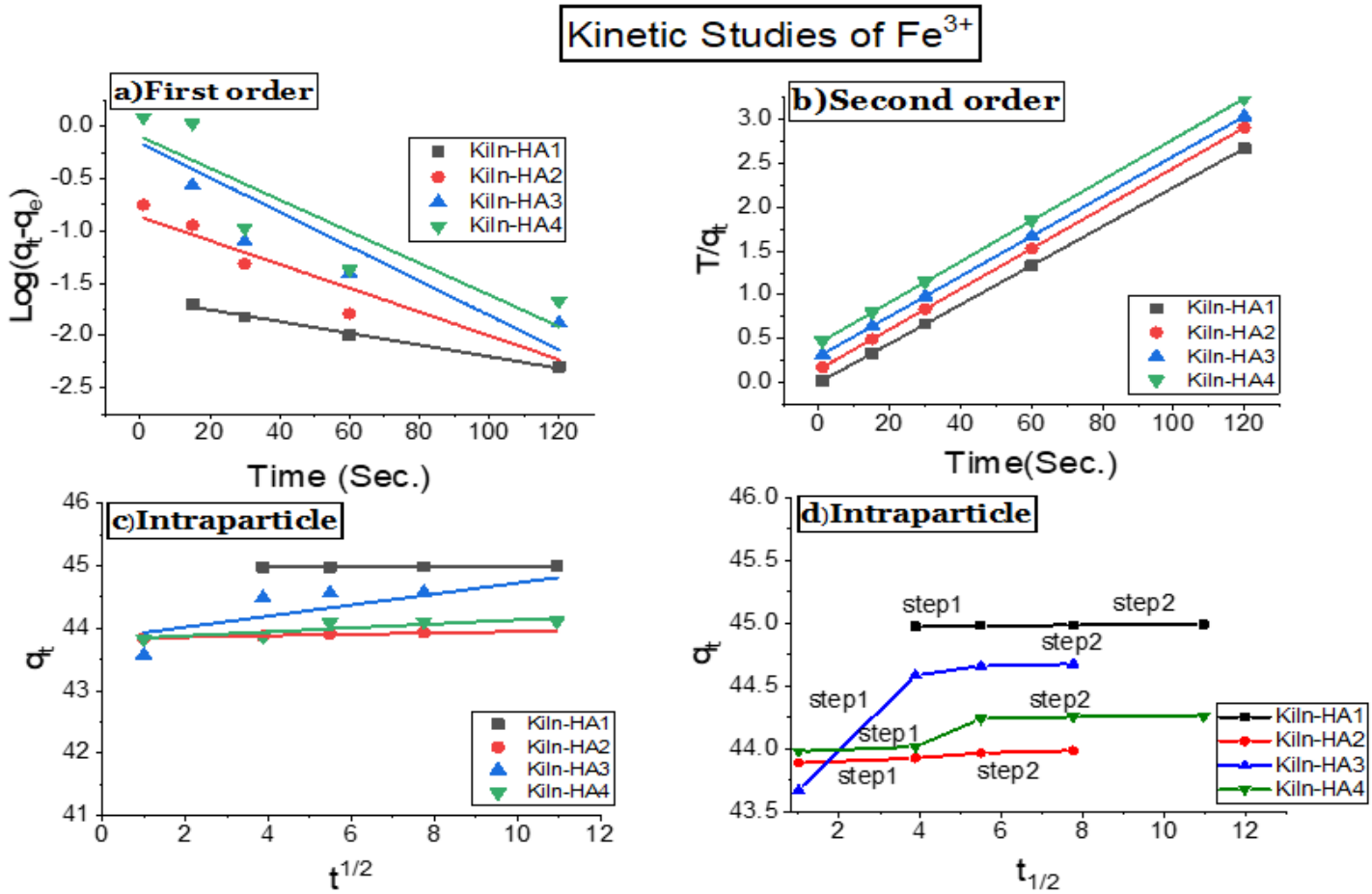

Figure 18

Kinetic Studies: I) pseudo-first, II) pseudo second and intra diffusion of Fe ions onto Hydroxyapatite

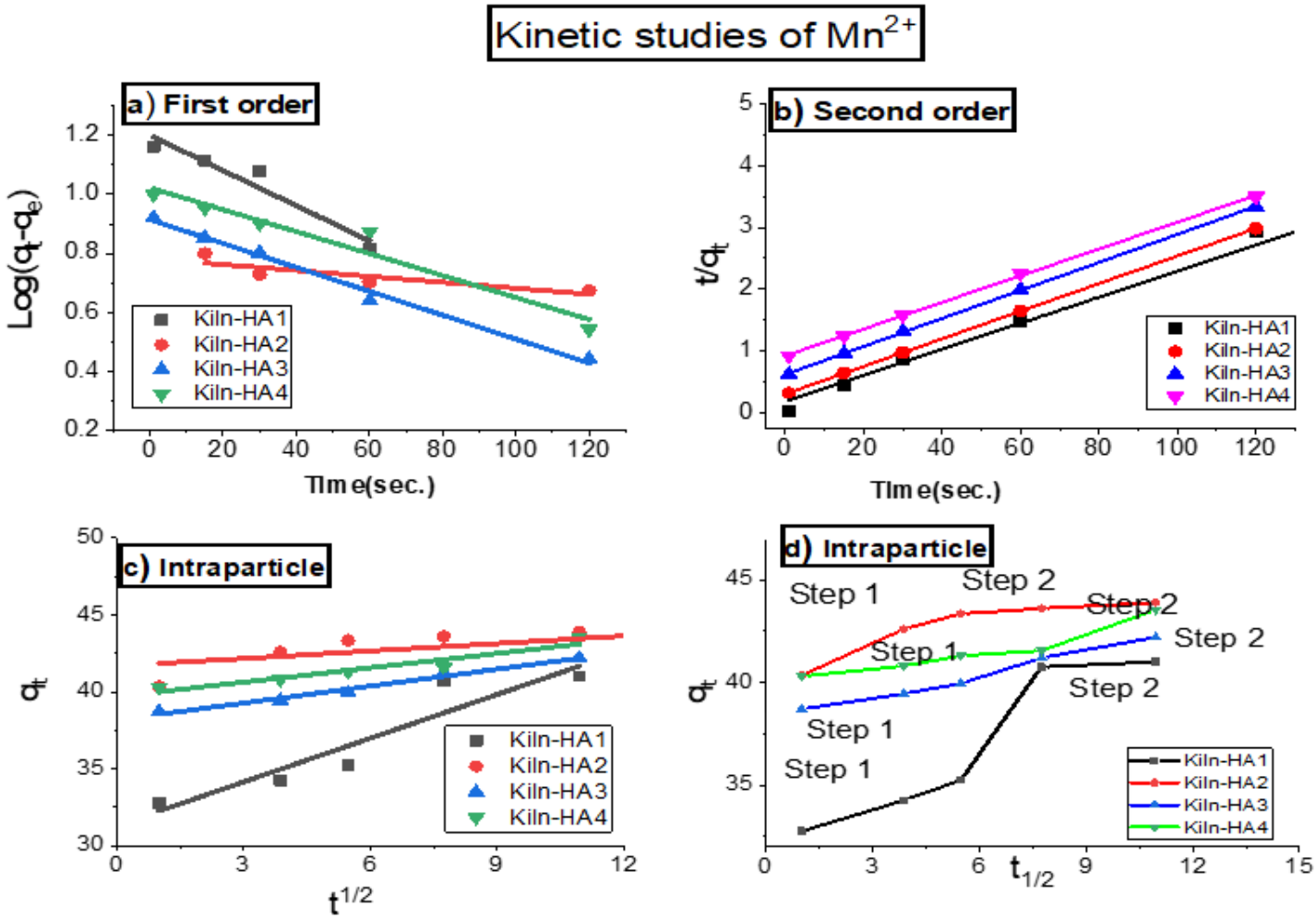

Figure 19

Kinetic Studies: I) pseudo-first, II) pseudo second and intra diffusion (III) of Mn ions onto Hydroxyapatite

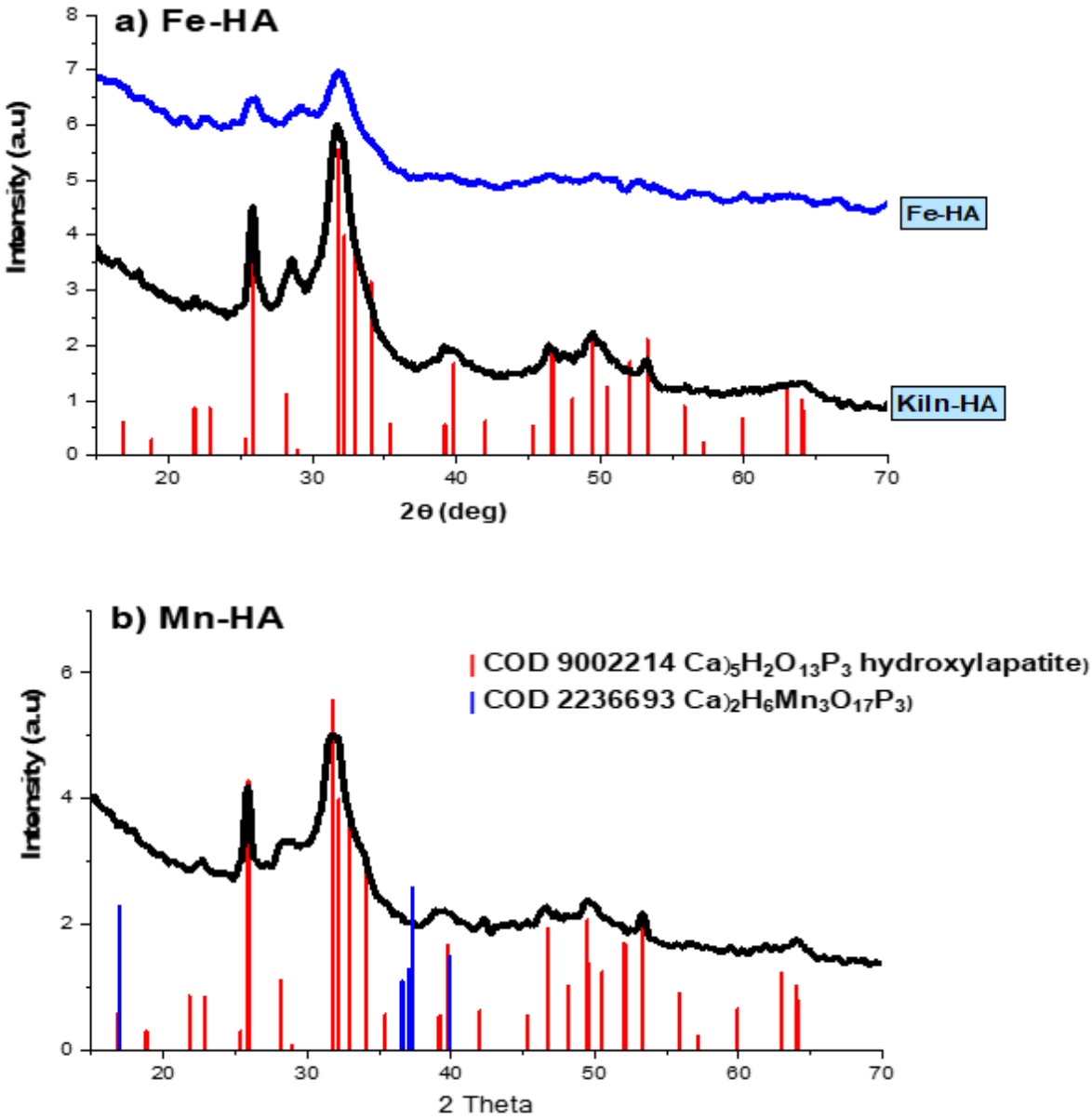

Figure 20

XRD of a) Fe3+loaded on Kiln-HA b) Mn2+ loaded on Kiln-HA

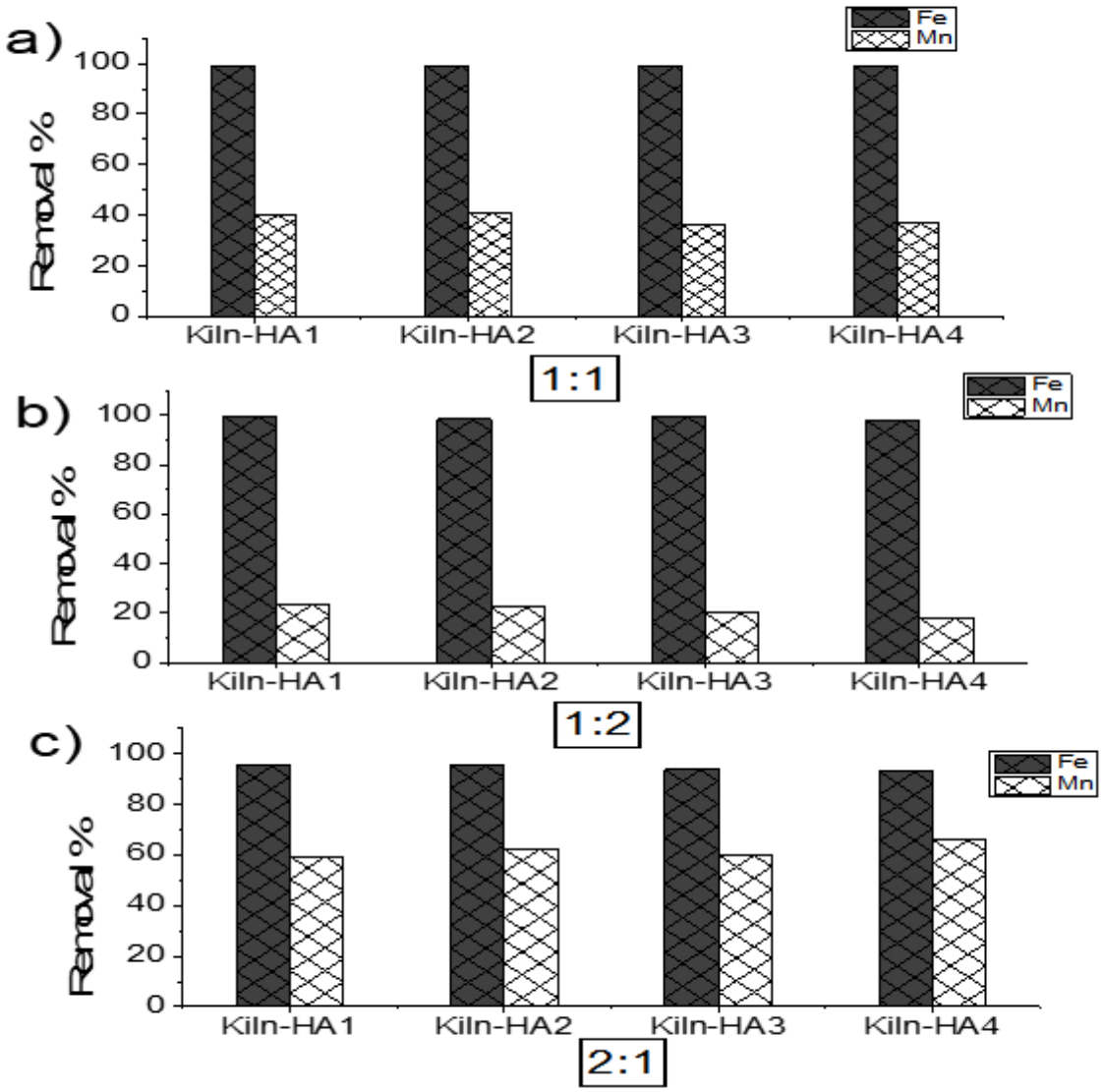

Figure 21

Competitive adsorption in Mixture Fe3+/Mn2+ a) 1:1 b)1:2 c) 2:1

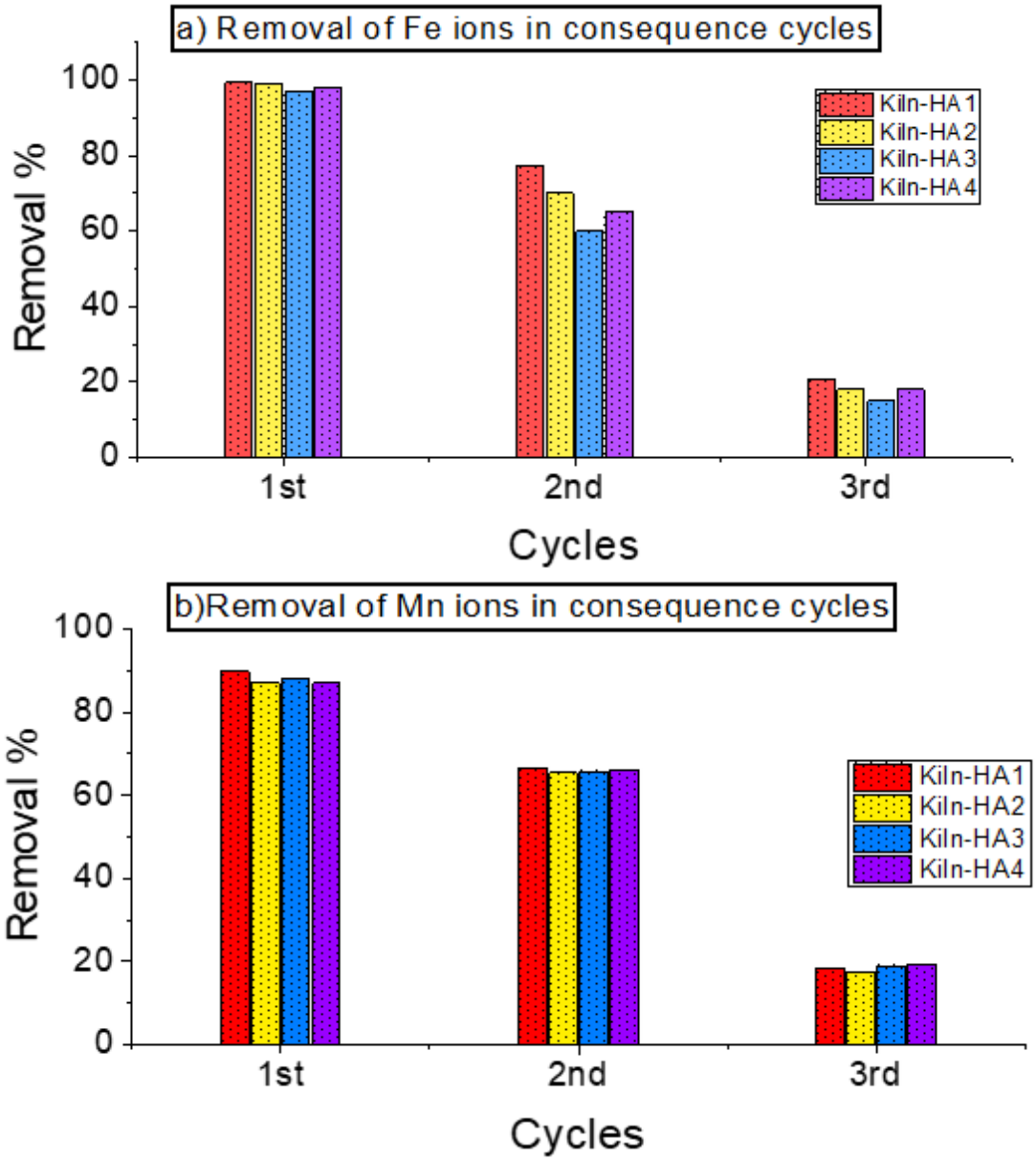

Figure 22

Removal of Fe3+ and Mn2+ ions in consequence cycles

Supplementary Files

This is a list of supplementary files associated with this preprint. Click to download.

- Graphicalabstract.docx